



ELSEVIER
ACADEMIC
PRESS

Non-Viral Vectors for Gene Therapy

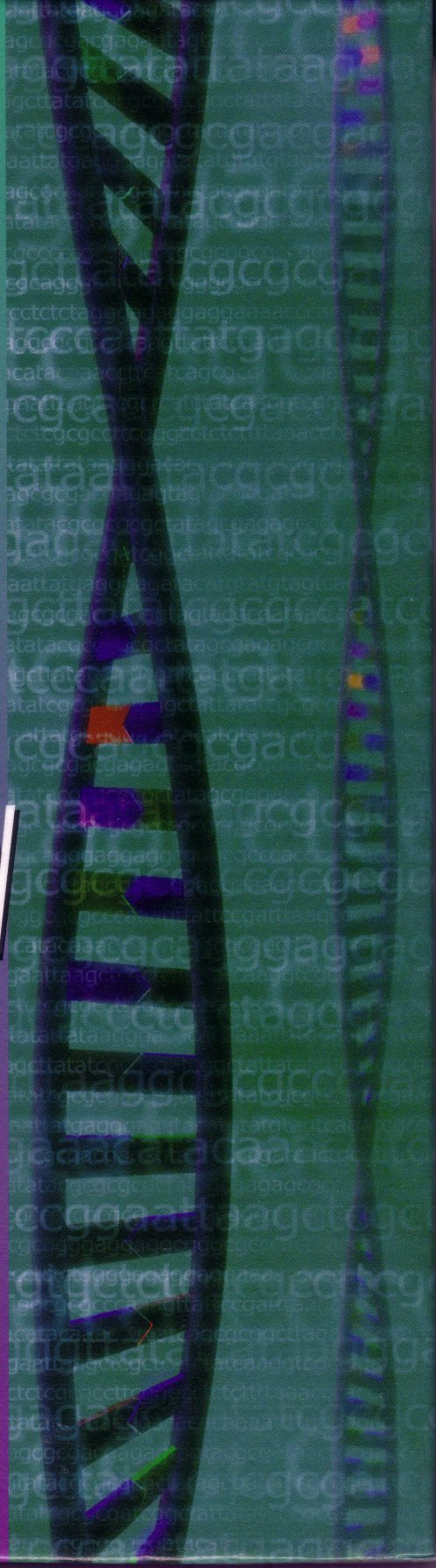
Second Edition: Part I

edited by

Leaf Huang

Mien-Chie Hung

Ernst Wagner



Lipoplex Structures and Their Distinct Cellular Pathways

Kai Ewert, Heather M. Evans, Ayesha Ahmad, Nelle L. Slack, Alison J. Lin, Ana Martin-Herranz, and Cyrus R. Safinya

Materials Department, Physics Department, and Molecular, Cellular and Developmental Biology Department, University of California, Santa Barbara Santa Barbara, California 93106

- I. Introduction
- II. Formation, Structures, and Stability of CL-DNA Complexes
 - A. Complex formation and structures
 - B. Overcharging and stability of lamellar CL-DNA complexes
- III. Structure-Transfection Efficiency Relationships of CL-DNA Complexes
 - A. Three-dimensional confocal imaging of CL-DNA complexes interacting with cells
 - B. The relationship between the membrane charge density of lamellar CL-DNA complexes and transfection efficiency
 - C. Transfection properties of new multivalent cationic lipids
 - D. A model of cell entry by L_{α}^C CL carriers: activated fusion, dependent on σ_M and elastic moduli of complex membranes
 - E. Transfection properties of inverted hexagonal H_{II}^C complexes
 - F. A model of cell entry by CL-vectors with the H_{II}^C structure: relevance of the outermost lipid layer
- IV. PEGylated CL-DNA Complexes: Surface Functionalization and Distinct DNA-DNA Interaction Regimes
 - A. DNA-DNA interaction regimes in PEGylated CL-DNA complexes
 - B. Surface functionalization of CL-DNA complexes with PEG-lipids

- V. Conclusion
- VI. Future Directions
- VII. Main Abbreviations
- Acknowledgments
- References

ABSTRACT

Cationic liposomes (CLs) are used as non-viral vectors in worldwide clinical trials of gene therapy. Among other advantages, CL-DNA complexes have the ability to transfer very large genes into cells. However, since the understanding of their mechanisms of action is still incomplete, their transfection efficiencies remain low compared to those of viruses. We describe recent studies which have started to unravel the relationship between the distinct structures and physicochemical properties of CL-DNA complexes and their transfection efficiency by combining several techniques: synchrotron X-ray diffraction for structure determination, laser-scanning confocal microscopy to probe the interactions of CL-DNA particles with cells, and luciferase reporter-gene expression assays to measure transfection efficiencies in mammalian cells. Most CL-DNA complexes form a multilayered structure with DNA sandwiched between the cationic lipids (lamellar complexes, L_{α}^C). Much more rarely, an inverted hexagonal structure (H_{II}^C) with single DNA strands encapsulated in lipid tubules is observed. An important recent insight is that the membrane charge density σ_M of the CL-vector, rather than, for example, the charge of the cationic lipid, is a universal parameter governing the transfection efficiency of L_{α}^C complexes. This has led to a new model of the intracellular release of L_{α}^C complexes, through activated fusion with endosomal membranes. In contrast to L_{α}^C complexes, H_{II}^C complexes exhibit no dependence on σ_M , since their structure leads to a distinctly different mechanism of cell entry. Surface-functionalized complexes with poly(ethyleneglycol)-lipids (PEG-lipids), potentially suitable for transfection *in vivo*, have also been investigated, and the novel aspects of these complexes are discussed. © 2005, Elsevier Inc.

I. INTRODUCTION

Gene delivery by synthetic (non-viral) vectors continues to attract the interest of a large number of research groups, motivated mainly by the promises of gene therapy (Chesnoy and Huang, 2000; Clark and Hersh, 1999; De Smedt *et al.*, 2000; Ewert *et al.*, 2004; Felgner and Rhodes, 1991; Ferber, 2001; Friedmann, 1997; Henry, 2001; Huang *et al.*, 1999; Kumar *et al.*, 2003; Mahato and Kim, 2002; Miller, 1998; Niidome and Huang, 2002; Wagner, 2004). Following initial

landmark studies (Felgner *et al.*, 1987; Nabel *et al.*, 1993; Wolff, 1994), cationic liposomes (CLs, closed bilayer membrane shells of lipid molecules) have been established as one of the most prevalent synthetic vectors. They are already used widely for *in vitro* transfection of mammalian cells in research applications, with numerous formulations commercially available (Miller, 2003). To enable the use of CL-DNA complexes in gene therapy, their mechanism of action is extensively investigated in many laboratories, concurrently with ongoing, mostly empirical, clinical trials (Edelstein *et al.*, 2004), for example, to develop cancer vaccines. Extensive and current information on clinical trials in the field of gene therapy is collected and made available at <http://www.wiley.co.uk/genetherapy/clinical/> (The Journal of Gene Medicine Clinical Trial Web site, 2004).

A key advantage of CLs over viral methods is the lack of a specific immune response, due to the absence of viral proteins. This was tragically emphasized by a recent, much publicized complication in clinical trials of viral vectors: a patient died due to an unanticipated, severe inflammatory response to an adenoviral vector (Raper *et al.*, 2003). Further emphasizing safety concerns, a successful trial that used retroviral vectors to treat children with severe combined immunodeficiency (SCID) (Cavazzana-Calvo *et al.*, 2000) faced a major setback when two patients (out of ten) developed a leukemia-like disease (Hacein-Bey-Abina *et al.*, 2003a), later confirmed to have resulted from insertional mutagenesis (Hacein-Bey-Abina *et al.*, 2003b). In addition, while viral capsids have a maximum DNA-carrying capacity of about 40 kbp (Friedmann, 1997), CL-DNA complexes place no limit on the size of the DNA, since the vector is formed by self-assembly (Koltover *et al.*, 1998; Lasic *et al.*, 1997; Rädler *et al.*, 1997). Thus, optimally designed CL-vectors offer the potential of delivering multiple human genes and regulatory sequences, extending over hundreds of thousands of DNA base-pairs. In fact, fractions of an artificial human chromosome, about 1 million base-pairs in size, have been transferred into cells using cationic lipids as a vector, albeit extremely inefficiently (Harrington *et al.*, 1997; Willard, 2000).

The main disadvantage of CL-based gene vectors is that their transfection efficiency (TE), which is a measure of the amount of successfully transferred and expressed DNA, remains much lower than that of viral vectors, particularly for *in vivo* applications (Miller, 2003). This has spurred intense research activity aimed at enhancing TE. For further improvement of the transfection efficiency of non-viral methods, it will be crucial to gain deep insight into their mechanism of transfection on the molecular and self-assembled level. This requires a complete understanding of the supramolecular structures of CL-DNA complexes, their interactions with cell membranes, the intracellular events leading to release of DNA for possible expression as well as the physical and chemical basis of these.

Our work investigates the mechanisms of transfection by CL-DNA complexes at the molecular to cellular level, focusing on the influence of the nanostructure of the complex and, within a given structure (L_{α}^C or H_{II}^C),

the physical (e.g., mechanical properties) and physico-chemical (e.g., charge density) parameters of the membranes forming the complex. To this end, a variety of techniques are employed: synchrotron X-ray diffraction (XRD) for structure determination (Koltover *et al.*, 1998, 1999, 2000; Lasic *et al.*, 1997; Lin *et al.*, 2000, 2003; Safinya, 2001; Salditt *et al.*, 1997; Rädler *et al.*, 1997), three-dimensional laser scanning confocal microscopy (LSCM) for imaging pathways and interactions of complexes within cells (Lin *et al.*, 2000, 2003) and reporter gene assays in animal cell culture (Lin *et al.*, 2000, 2003; Ewert *et al.*, 2002) for quantifying TE. By combining these characterization methods, the distinct interactions between cells and high and low transfection efficiency complexes, as observed in confocal microscopy, can be rationalized on the basis of the structure and properties of the complexes (Safinya and Koltover, 1999; Safinya *et al.*, 2002; Tranchant *et al.*, 2004). Unless otherwise stated, experiments reviewed in this chapter used mouse fibroblast L-cells, a luciferase reporter gene assay and complexes at a lipid-to-DNA charge ratio (ρ_{chg}) of 2.8, which corresponds to the middle of a plateau region observed when plotting TE as a function of increasing ρ_{chg} above the isoelectric point (Lin *et al.*, 2003).

The structures of most lipids mentioned in this chapter are shown in Fig. 5.1. As neutral lipids, 1,2-dioleoyl-*sn*-glycerophosphatidylethanolamine (DOPE) and 1,2-dioleoyl-*sn*-glycerophosphatidylcholine (DOPC) were employed. DOPE is one of the main neutral lipids currently in use in gene therapy applications of CLs. The cationic lipids were either commercially available (DOTAP), gifts from other investigators (DMR1E, DOSPA) or synthesized in our group (PEG-lipids, MVLs (Table 5.1)).

The *in vitro* studies described here apply mainly to TE optimization in *ex vivo* cell transfection, where cells are removed and returned to patients after transfection. In particular, an improved understanding of the key mechanisms of transfection in continuous cell lines should aid clinical efforts to develop efficient CL-vector cancer vaccines in *ex vivo* applications, which induce transient expression of genes encoding immuno-stimulatory proteins (Clark and Hersh, 1999; Ferber, 2001; Nabel *et al.*, 1993; Rinehart *et al.*, 1997; Stopeck *et al.*, 1998).

II. FORMATION, STRUCTURES, AND STABILITY OF CL-DNA COMPLEXES

CL-DNA complexes readily form for a large variety of lipids. This ease of preparation and the variability of the lipid composition constitute two of their main advantages. In this section, we discuss findings relevant to understanding the formation, nanostructure and thermodynamic stability of CL-DNA complexes.

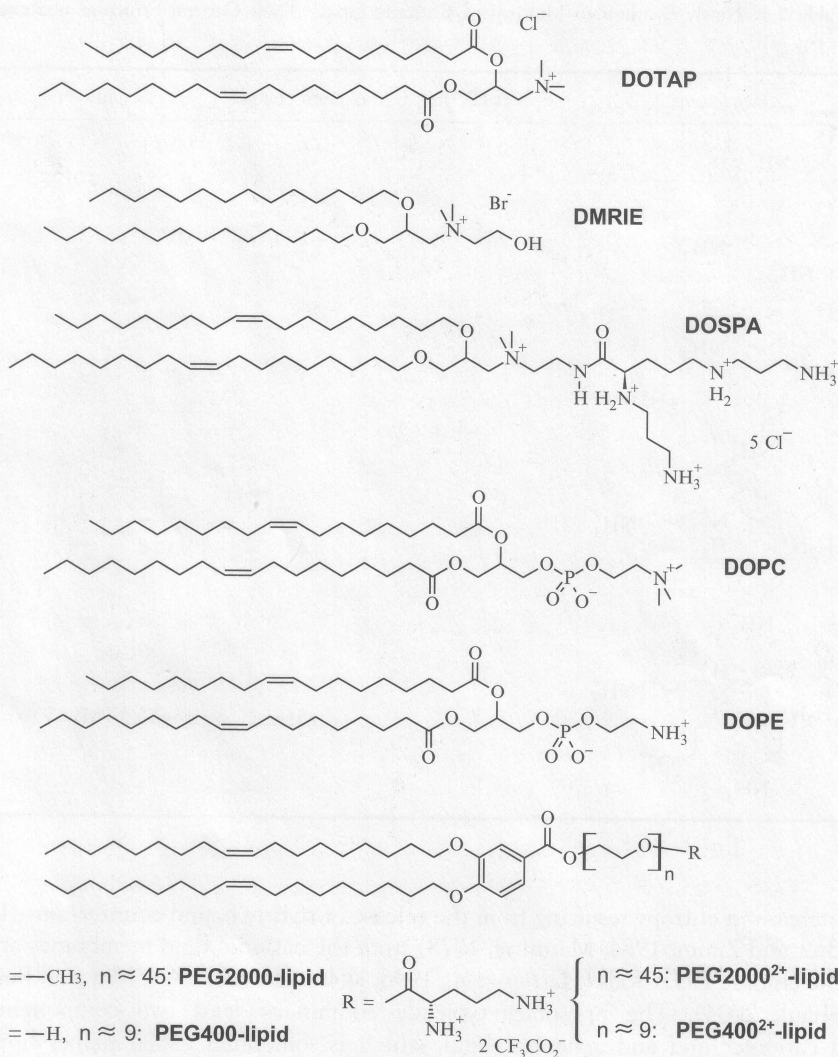

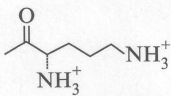
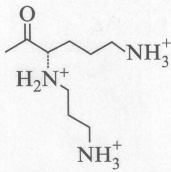
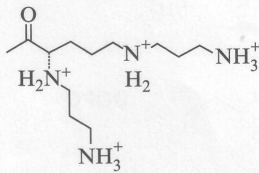
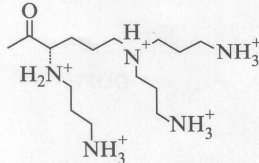


Figure 5.1. Chemical structures and abbreviated names of cationic and neutral lipids mentioned in this chapter.

A. Complex formation and structures

Combining solutions of cationic liposomes and DNA results in their spontaneous self-assembly into small (0.2 μm diameter) globular particles of CL-DNA complexes. This is schematically illustrated in Fig. 5.2. Depending on the conditions of formation, the initially formed particles may aggregate to form much larger assemblies. The driving force for complex formation is a large

Table 5.1. Newly Synthesized Multivalent Cationic Lipids. Their General Structure is Shown in Fig. 5.10

Headgroup	Spacer (EO) _n	Maximum charge	Lipid name
	0	+1	MVL1
	0	+2	MVL2
	0	+3	MVL3
	0	+4	MVL4
	0, 2	+5	MVL5 / TMVL5 (n=2)

increase in entropy resulting from the release of tightly bound counter-ions (Le Bret and Zimm, 1984; Manning, 1978) from the cationic lipid membranes and the anionic DNA rods (Harries *et al.*, 1998; Koltover *et al.*, 1999; May and Ben-Shaul, 2004). The liposomes typically contain at least two components: a cationic lipid and a neutral lipid, which is sometimes called helper lipid. Depending on the ratio of charges on the cationic lipid and the DNA (ρ_{chg}), anionic, neutral or cationic complexes are obtained. We refer to neutral complexes, where the charges on the DNA exactly match those on the cationic lipids ($\rho_{\text{chg}} = 1$), as isoelectric. For transfection, positively charged ($\rho_{\text{chg}} > 1$) complexes are used, since the initial attachment of CL-DNA complexes to mammalian cells is mediated by electrostatic attractions between the complexes and negatively charged cell surface proteoglycans (Kopatz *et al.*, 2004; Mislick and Baldeschwieler, 1996; Mounkes *et al.*, 1998).

Synchrotron X-ray diffraction experiments have solved the two types of structures observed in CL-DNA complexes. Shown schematically on the right in

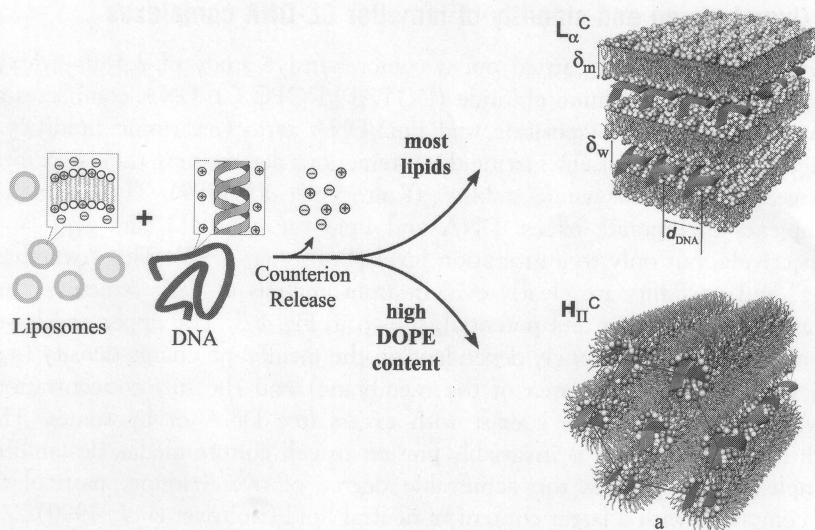


Figure 5.2. Schematic depiction of the formation and the nanostructures of CL-DNA complexes. Counterions are tightly bound to the charged surfaces of DNA and CLs (Manning condensation: Manning, 1978). The entropy gained from their release provides the main driving force for the self-assembly into distinctly structured complexes. The schematics on the right show the local interior structure of CL-DNA complexes for the two structures observed to date, as derived from synchrotron X-ray diffraction data. Neutral and cationic lipids are depicted as having white and gray headgroups, respectively. Top: The most commonly observed lamellar phase (denoted L_{α}^C), consisting of alternating lipid bilayers and DNA monolayers. The interlayer spacing is $d = \delta_w + \delta_m$. Bottom: Few lipid mixtures produce the inverted hexagonal phase of CL-DNA complexes (denoted H_{II}^C), which is comprised of lipid-coated DNA strands arranged on a hexagonal lattice. Schematics reprinted with permission from Koltover *et al.* (1998).

Fig. 5.2, these are a multilamellar structure with DNA monolayers sandwiched between cationic membranes (L_{α}^C) (Lasic *et al.*, 1997; Rädler *et al.*, 1997) and an inverted hexagonal structure with DNA encapsulated within cationic lipid monolayer tubes (H_{II}^C) (Koltover *et al.*, 1998). Earlier work succeeded in elucidating the parameters which control the structure of the complex: the inverted hexagonal phase is observed for higher contents of DOPE, which has a negative spontaneous curvature (Israelachvili, 1992), as well as for complexes whose membranes have been softened by the addition of cosurfactant (Koltover *et al.*, 1998).

In lamellar CL-DNA complexes, the DNA monolayers, sandwiched between lipid bilayers, are ordered with a well-defined separation distance d_{DNA} between adjacent DNA rods (Koltover *et al.*, 2000; Rädler *et al.*, 1997). By tuning the charge density of the membranes or introducing PEG-lipids, this DNA distance can be adjusted between 25 Å and 60 Å (see below).

B. Overcharging and stability of lamellar CL-DNA complexes

Koltover *et al.* (1999) carried out a comprehensive study of 2,3-dioleoyloxypropyltrimethylammonium chloride (DOTAP)/DOPC CL-DNA complexes as a function of lipid composition and lipid/DNA ratio (ρ : cationic lipid/DNA weight ratio), aimed at elucidating the interactions determining their structure, charge, and thermodynamic stability (Koltover *et al.*, 1999). These lamellar complexes incorporate excess DNA and lipid for $\rho_{\text{chg}} < 1$ and $\rho_{\text{chg}} > 1$, respectively, but only to a saturation level (Bruinsma, 1998). This “overcharging” and its limits are clearly evident from analysis of their structures and measurements of their zeta potential, shown in Fig. 5.3. The upper and lower saturation levels are strongly dependent on the membrane charge density (σ_M , the average charge per area of the membrane) and the salt concentration. Beyond them, complexes coexist with excess free DNA or liposomes. The addition of salt, which is invariably present in cell culture media, destabilizes complexes and reduces the achievable degree of overcharging, particularly for complexes with a larger content of neutral lipid (Koltover *et al.*, 1999).

The stability of CL-DNA complexes is an important parameter, since DNA eventually needs to be released in order to become transcriptionally active. The biogenic polycations spermidine³⁺ and spermine⁴⁺, which are known to be present at mM conditions in the cytosol during the cell cycle, are able to remove DNA from the CL-DNA complexes to form hexagonally packed DNA-polyamine particles in bulk solution (Koltover *et al.*, 2000). This suggests one possible mechanism for intracellular release of DNA from CL-DNA complexes during transfection. Once removed from the CL-DNA complex, the DNA can easily dissociate from the short polyamine molecules, since the probability of DNA dissociating from an oppositely charged oligo-electrolyte increases with decreasing oligo-electrolyte length. Not surprisingly, *in-vitro* X-ray studies also show that histones are able to remove DNA from CL-DNA complexes (Evans H., and Safinya C. R., 2001, unpublished results).

Negatively charged proteins are another cellular component that is likely involved in the dissociation of CL-DNA complexes in the cytoplasm. Synchrotron X-ray diffraction has solved the structure of CL-complexes of poly(L-glutamic acid) (PGA) (Subramanian *et al.*, 2000), a negatively charged model polypeptide, as well as F-actin, a highly abundant anionic cytoskeletal protein (Wong *et al.*, 2000). The data for the lipid-PGA complexes are consistent with a “pinched lamellar” phase, shown schematically in Fig. 5.4 (left). In this structure, PGA and the cationic lipid associate to form localized “pinched” regions. Between “pinches”, pockets of water are stabilized with a large equilibrium spacing of 60 Å due to hydration repulsion of neutral bilayers.

CL-F-actin complexes consist of a network of flattened multilamellar tubules with an average width of $\approx 0.25 \mu\text{m}$. The tubules are formed from stacks of triple-layers consisting of a lipid bilayer sandwiched between two monolayers

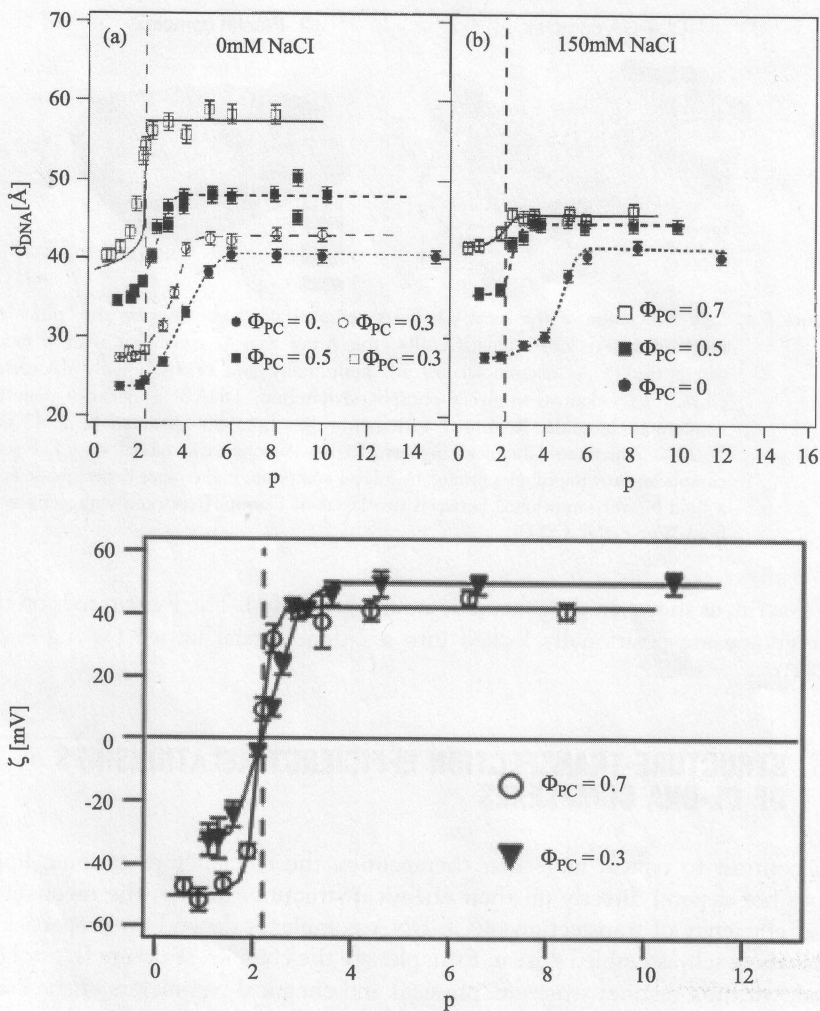


Figure 5.3. Top: (a) Variation of the DNA interaxial distance d_{DNA} with lipid/DNA weight ratio (ρ) in DOPC/DOTAP/DNA-complexes at a constant weight fraction of DOPC (Φ_{PC}), prepared in deionized water. The vertical dashed line indicates the isoelectric point ($\rho = 2.2$). The solid line through the data at $\Phi_{DOPC} = 0.7$ is the result of nonlinear Poisson–Boltzman theory for complexes with low membrane charge density (Bruinsma, 1998). The dashed lines are guides to the eye. The complexes are single-phase in the region of increasing d_{DNA} , coexisting with DNA at lower ρ and with lipid at higher ρ . (b) Same as (a) at 150 mM NaCl. All lines are guides to the eye. Bottom: Variation of the complexes' ζ -potential with changing ρ . The vertical line marks the isoelectric point. Lines through the data are a guide to the eye. Reprinted with permission from Koltover *et al.* (1999). © 1999 Biophysical Society.

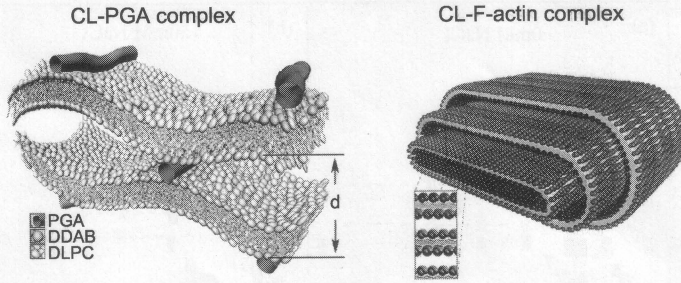


Figure 5.4. Left: Schematic of the local CL-PGA complex structure, showing the “pinching” mechanism. At larger length scales, the X-ray data is consistent with a model where the PGA macromolecules are positionally and orientationally disordered. DLPC: 1,2-Dilauroyl-*sn*-glycerophosphatidylcholine; DDAB: Didodecyl dimethyl ammonium bromide. Reprinted with permission from Subramanian *et al.* (2000). © 2000 American Chemical Society. Right: A schematic model of CL-F-actin complexes showing tubules formed by 3-layer composite membranes (inset) made up of a lipid bilayer sandwiched between two layers of F-actin. Reprinted with permission from Wong *et al.* (2000).

of F-actin, as shown in the schematic in Fig. 5.4 (right). The F-actin rods on the membrane are positionally locked into a 2-dimensional lattice (Wong *et al.*, 2000).

III. STRUCTURE-TRANSFECTION EFFICIENCY RELATIONSHIPS OF CL-DNA COMPLEXES

In contrast to typical molecular therapeutics, the efficiency of cationic lipids does not depend directly on their chemical structure. Rather, the mechanism and efficiency of transfection of CL-DNA complexes depend on properties of the whole self-assembled system. Examples are the complex structure (L_{α}^C or H_{II}^C) and, within a distinct structure, physical and chemical parameters of the complexes, such as the lipid/DNA charge ratio or the lipid composition. A lipid-independent measure of the ratio of neutral to cationic lipid is the membrane charge density (σ_M), the average charge per unit area of membrane. For isoelectric CL-DNA complexes in the L_{α}^C phase and d_{DNA} larger than the diameter of DNA with one hydration layer, d_{DNA} can directly be calculated from the average distance per anionic charge along the DNA backbone (l_0), and the membrane charge density σ_M : $d_{DNA} = \epsilon / (l_0 \sigma_M)$ (Koltover *et al.*, 1999; Rädler *et al.*, 1997). Thus, the DNA interaxial spacing, which can be measured by X-ray diffraction, is a measure of σ_M , decreasing as the membrane charge density increases. For positively charged complexes ($\rho_{chg} > 1$), σ_M can no longer be directly calculated from d_{DNA} , but the same qualitative relationship still holds.

Early experiments in our group varied σ_M systematically for lamellar and inverted hexagonal phases of CL-DNA complexes to investigate the effect on TE and, via confocal microscopy, the pathways of gene delivery. Prior to those studies, TE measurements by other groups had shown that in mixtures of the monovalent cationic lipid DOTAP and neutral lipids, typically at a weight ratio between 1:1 and 1:3, DOPE aided transfection while DOPC severely suppressed it (Farhood *et al.*, 1995; Hui *et al.*, 1996). Therefore, it seemed that DOPE-based H_{II}^C complexes always transfect more efficiently than L_{α}^C complexes. The findings described below, from investigations on DNA complexes covering the whole range of compositions of DOTAP with neutral DOPC and DOPE, show that the difference in performance between the two types of complexes is more subtle than previously believed and that there are regimes of composition where the TE of complexes in the L_{α}^C phase rivals that of the best H_{II}^C complexes.

The striking difference in TE between L_{α}^C and H_{II}^C complexes at a cationic to neutral lipid ratio of 1:2 is illustrated in Fig. 5.5. Lamellar and inverted hexagonal complexes were prepared from DOTAP/DOPC and DOTAP/DOPE mixtures, respectively. Synchrotron XRD scans of complexes with plasmid DNA, measured in Dulbecco's Modified Eagle Medium (DMEM), a common cell culture medium, are shown in Fig. 5.5. Schematic views of the structures are also pictured (Lin *et al.*, 2000, 2003). The DOTAP/DOPC complexes at a molar fraction $M_{DOPC} = 0.67$ (Fig. 5.5, left)

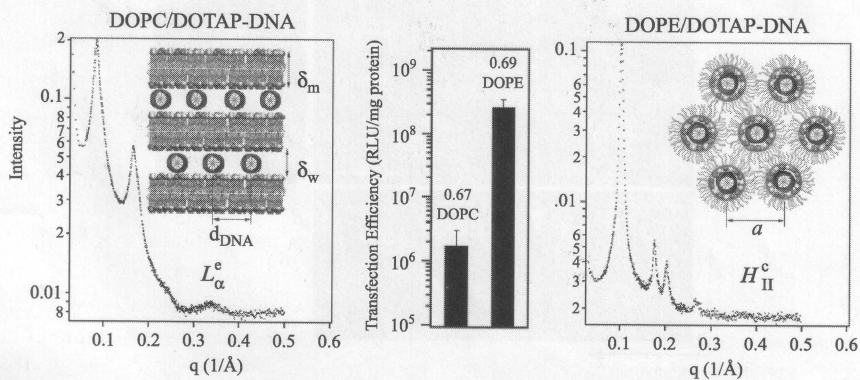


Figure 5.5. Comparison of CL-DNA complex structure and transfection efficiency for a cationic to neutral lipid ratio of $\approx 1:2$. Complexes were prepared using pGL3 plasmid DNA and DOTAP as the cationic lipid. Left: Small angle X-ray scattering pattern and schematic view (inset) of lamellar L_{α}^C complexes (molar fraction $M_{DOPC} = 0.67$). Right: Small angle X-ray scattering pattern and schematic view (inset) of inverted hexagonal H_{II}^C complexes ($M_{DOPE} = 0.69$). Middle: TE of the complexes. Note the logarithmic scale. Reprinted with permission from Lin *et al.* (2003). © 2003 Biophysical Society.

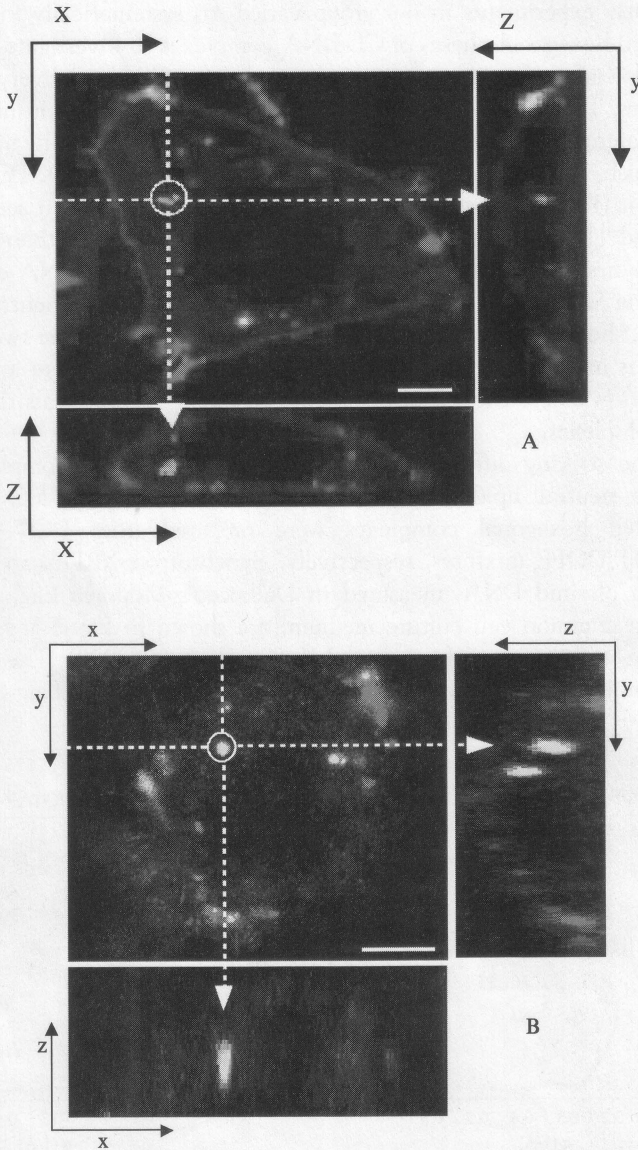
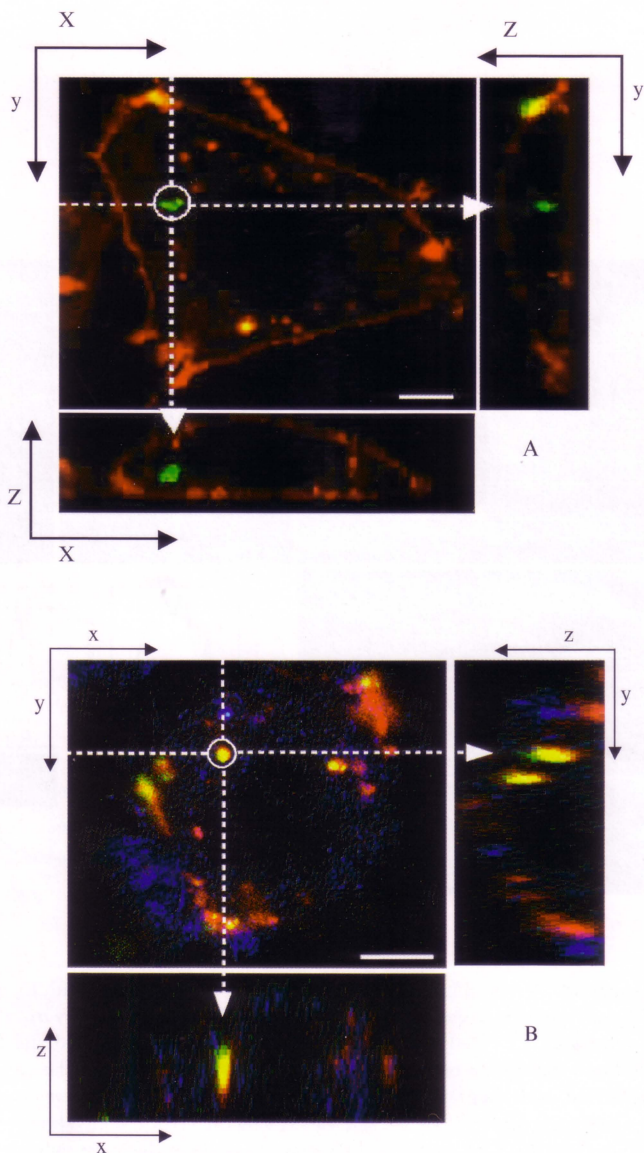


Figure 5.6. Laser scanning confocal microscopy images of transfected mouse L cells, fixed six hours after incubation with complexes. For each set of images, the center image is the x-y (top) view at a given z; the right shows a y-z side view along the vertical dotted line; and the bottom a x-z side view along the horizontal dotted line. Red and green fluorescence corresponds to lipid and DNA labels, respectively; yellow, the overlap of the two, denotes CL-DNA complexes. Scale bars are 5 μm . (A): Cells transfected with $\text{H}_{\text{II}}^{\text{C}}$ complexes ($M_{\text{DOPE}} = 0.69$) show transfer of fluorescent lipid to the cell plasma



Chapter 5, Figure 5.6. Laser scanning confocal microscopy images of transfected mouse L cells, fixed six hours after incubation with complexes. For each set of images, the center image is the x - y (top) view at a given z ; the right shows a y - z side view along the vertical dotted line; and the bottom a x - z side view along the horizontal dotted line. Red and green fluorescence corresponds to lipid and DNA labels, respectively; yellow, the overlap of the two, denotes CL-DNA complexes. Scale bars are $5 \mu\text{m}$. (A): Cells transfected with H_{II}^C complexes ($M_{\text{DOPE}} = 0.69$) show transfer of fluorescent lipid to the cell plasma membrane and the release of DNA (green; in the circle) within the cell. (B): LSCM image of cells transfected with L_{α}^C complexes at $M_{\text{DOPC}} = 0.67$, where TE is low, as shown in Figure 5.5. The cell outline was observed in reflection mode, appearing in blue. No evidence for fusion is visible and intact CL-DNA complexes such as the one marked by a circle are observed inside the cells. This observation implies that DNA remains trapped within the complexes, consistent with the observed low transfection efficiency. Reprinted with permission from Lin *et al.* (2003). © 2003 Biophysical Society.

showed sharp peaks at $q_{001} = 0.083 \text{ \AA}^{-1}$, $q_{002} = 0.166 \text{ \AA}^{-1}$, with a shoulder peak at $q_{003} = 0.243 \text{ \AA}^{-1}$ and $q_{004} = 0.335 \text{ \AA}^{-1}$, resulting from the layered structure of the L_{α}^C phase. The interlayer spacing is $d = \delta_m + \delta_w = 2\pi/q_{001} = 75.70 \text{ \AA}$ (cf. Fig. 5.2). For DOTAP/DOPE complexes at $M_{\text{DOPE}} = 0.69$, small angle X-ray scattering (Fig. 5.5, right) revealed four orders of Bragg peaks at $q_{10} = 0.103 \text{ \AA}^{-1}$, $q_{11} = 0.178 \text{ \AA}^{-1}$, $q_{20} = 0.205 \text{ \AA}^{-1}$ and $q_{21} = 0.270 \text{ \AA}^{-1}$, denoting the H_{II}^C phase with a unit cell spacing $a = 4\pi/[(3)^{1/2}q_{10}] = 70.44 \text{ \AA}$ (cf. Fig. 5.2). The results of TE experiments, shown in Fig. 5.5 (middle), demonstrate that the TE attainable with complexes in the H_{II}^C phase at $M_{\text{DOPE}} = 0.69$ is by more than two decades higher than that of L_{α}^C complexes at $M_{\text{DOPC}} = 0.67$.

A. Three-dimensional confocal imaging of CL-DNA complexes interacting with cells

To explore the structure–function correlation in more detail, we examined the transfer of CL-DNA complexes into cells and the subsequent DNA release by LSCM, which allows determining the position of objects relative to cells with certainty. The complexes were doubly tagged with fluorescent labels, Texas Red-DHPE for lipid and a covalently attached green for DNA (Mirus Label IT) (Lin *et al.*, 2003). Fig. 5.6 shows LSCM micrographs of mouse L cells, fixed six hours after the addition of complexes. In Fig. 5.6A, a typical image of a cell transfected with H_{II}^C complexes at $M_{\text{DOPE}} = 0.69$ is displayed. The lipid fluorescence clearly outlines the plasma membrane. Thus, either spontaneous transfer of labeled lipid or fusion of lipid with the plasma membrane has taken place. This may have occurred before or after entry through the endocytic pathway (Wrobel and Collins, 1995; Xu and Szoka 1996; Zabner *et al.* 1995, 1996). Inside the cell, both an aggregate of complexes (yellow) as well as lipid-free DNA (green) are visible. Thus, the interaction between H_{II}^C complexes and cells leads to the release of DNA from the CL-vector, consistent with the measured high TE.

Fig. 5.6B shows a corresponding confocal image for L_{α}^C complexes at $M_{\text{DOPC}} = 0.67$. In contrast to H_{II}^C complexes, no free DNA is visible. Instead, several intact CL-DNA complexes are found inside of the cell. One of these is highlighted in Fig. 5.6B. The complexes likely entered the cells through

membrane and the release of DNA (green; in the circle) within the cell. (B): LSCM image of cells transfected with L_{α}^C complexes at $M_{\text{DOPC}} = 0.67$, where TE is low, as shown in Figure 5.5. The cell outline was observed in reflection mode, appearing in blue. No evidence for fusion is visible and intact CL–DNA complexes such as the one marked by a circle are observed inside the cells. This observation implies that DNA remains trapped within the complexes, consistent with the observed low transfection efficiency. Reprinted with permission from Lin *et al.* (2003). © 2003 Biophysical Society. (See Color Insert.)

endocytosis: there is no fluorescent lipid observed in the cell membrane, ruling out cell entry via fusion. Cell entry by endocytosis has also been observed by others (Wrobel and Collins, 1995; Xu and Szoka 1996; Zabner *et al.* 1995). This was corroborated by LSCM images of cells prepared at 4°C, where endocytosis is inhibited. In this case, complexes were found attached to the outside cell surface, but not within the cell body (Lin *et al.*, 2000). Thus, LSCM shows that at $M_{\text{DOPC}} = 0.67$, most of the DNA remains trapped in the endosome with the CL-vector, consistent with the observed low TE.

B. The relationship between the membrane charge density of lamellar CL-DNA complexes and transfection efficiency

In further transfection experiments, an unexpected enhancement of TE by two decades took place as the concentration of DOPC in lamellar CL-DNA complexes was decreased. The dependence of TE on M_{DOPC} for the whole range of compositions resulting in single-phase DOPC/DOTAP-DNA complexes is shown in Fig. 5.7A (diamonds). It is important to note that all TE measurements were done with 2 μg of plasmid DNA at constant $\rho_{\text{chg}} = 2.8$. Thus, every data point used an identical amount of charged species (DNA and cationic lipid) and M_{DOPC} was varied solely by adjusting the amount of neutral lipid. The efficiency starts low for $0.5 < M_{\text{DOPC}} < 0.7$, increasing dramatically to a value, at $M_{\text{DOPC}} = 0.2$, which rivals that achieved by DOPE/DOTAP-DNA $\text{H}_{\text{II}}^{\text{C}}$ complexes. Similar results were obtained for another univalent cationic lipid, 2,3-di(myristyloxy)propyl(2-hydroxyethyl)dimethylammonium bromide (DMRIE), as also shown in Fig. 5.7A (triangles). However, a striking difference, which holds the key to a deeper understanding of the observed TE trends, was seen for the multivalent cationic lipid 2,3-Dioleyloxy-*N*-[2-(sperminecarboxamido)ethyl]-*N,N*-dimethyl-1-propylammonium chloride (DOSPA) as the cationic lipid (Fig. 5.7A, squares). A qualitatively similar curve is obtained, with TE decreasing rapidly above a critical M_{DOPC}^* . However, this M_{DOPC}^* is shifted from ≈ 0.2 , as observed for DOTAP and DMRIE complexes, to 0.7 ± 0.1 for DOSPA.

The main difference between DOSPA and the other lipids are their headgroups (Fig. 5.7, inset): DOSPA has a charge of up to +5 at a headgroup size that is only somewhat larger than that of DOTAP. Thus, the charge density (charge per area) of the headgroup is much higher for DOSPA. Consequently, the membrane charge density σ_{M} at a given M_{DOPC} is also significantly larger in complexes containing DOSPA than in complexes prepared from DOTAP or DMRIE.

Utilizing this insight, Fig. 5.7B shows the same TE data as Fig. 5.7A, now plotted against σ_{M} . Given the complexity of the CL-DNA-cell system and the fact that all other parameters are fixed by the experiment or the chemical structure, it is remarkable that the data for monovalent and multivalent lipids,

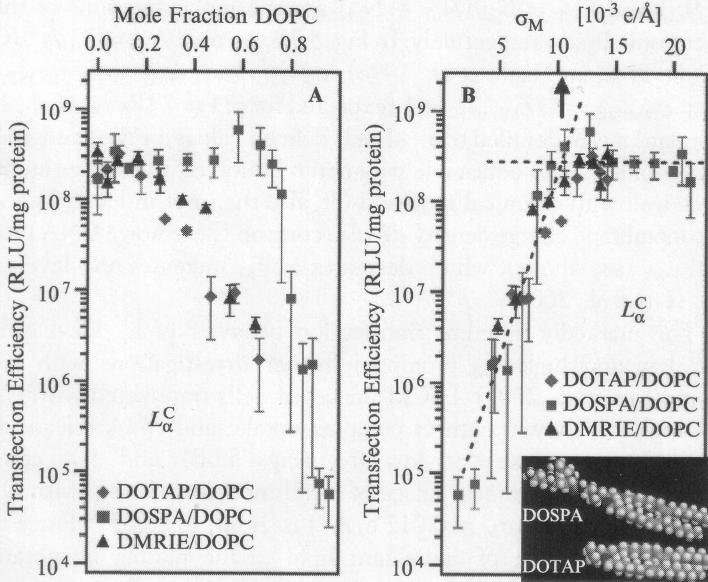


Figure 5.7. (A) Transfection efficiency, plotted as a function of varying molar fraction DOPC for complexes of the cationic lipids DOSPA, DOTAP, and DMRIE. (B) TE plotted versus the membrane charge density σ_M , demonstrating universal behavior of complexes containing cationic lipids with different charge and head group area (inset). For all three lipid systems, TE increases with σ_M up to an optimal σ_M^* , where it plateaus. An arrow marks $\sigma_M^* \approx 0.0104 \text{ e}/\text{\AA}^2$, determined by the intersection of two straight lines that were fit to the data (dashed lines). Note that the amount of transferred DNA was constant for all data points. Due to the fixed ρ_{chg} of 2.8, the same is true for the number of cationic charges on the lipids. The charge density was varied solely by varying the amount of neutral lipid. Reprinted with permission from Lin *et al.* (2003). © 2003 Biophysical Society.

spread out when plotted as a function of molar fraction of DOPC, coalesce into a single, universal curve as a function of σ_M . TE varies exponentially over nearly four decades as σ_M increases by a factor of ≈ 8 (Fig. 5.7B, σ_M between $0.0015 \text{ e}/\text{\AA}^2$ and $0.012 \text{ e}/\text{\AA}^2$) and the universal TE curve saturates beyond a common optimal $\sigma_M^* \approx 0.0104 \pm 0.0017 \text{ e}/\text{\AA}^2 \approx \text{e}/(100 \text{\AA}^2)$, indicated by an arrow in Fig. 5.7B. This clearly implies that σ_M is an important and universal parameter for transfection by lamellar CL-DNA complexes. The membrane charge density was calculated as

$$\begin{aligned} \sigma_M &= \text{total charge}/\text{total area} = eZN_{\text{cl}}/(N_{\text{nl}}A_{\text{nl}} + N_{\text{cl}}A_{\text{cl}}) \\ &= [1 - M_{\text{nl}}/(M_{\text{nl}} + rM_{\text{cl}})]\sigma_{\text{cl}} \end{aligned} \quad (5.1)$$

Here, $r = A_{\text{cl}}/A_{\text{nl}}$ is the ratio of the headgroup areas of cationic and neutral lipid; $\sigma_{\text{cl}} = eZ/A_{\text{cl}}$ is the charge density of the cationic lipid with valence Z ; $M_{\text{nl}} = N_{\text{nl}}/$

$(N_{nl} + N_{cl})$ and $M_{cl} = N_{cl}/(N_{nl} + N_{cl})$ are the molar fractions of the neutral and cationic lipids, respectively. In Fig. 5.7B, we used $A_{nl} = 72 \text{ \AA}^2$ (Gruner *et al.*, 1988; Tristram-Nagle *et al.*, 1998), $r_{DOTAP} = r_{DMRIE} = 1$, $r_{DOSPA} = 2$, $Z_{DOTAP} = Z_{DMRIE} = 1$, $Z_{DOSPA} = 4$ (expected for $\text{pH} \approx 7$ (Remy *et al.*, 1994)). Since standard methods failed to yield well-defined values for the headgroup area of cationic lipids, r is an adjustable parameter. However, the values used in the plots agree well with chemical intuition (cf. also the inset in Fig. 5.7). Interestingly, the membrane charge density σ_M also controls the average DNA interaxial spacing d_{DNA} (see above), which decreases as σ_M increases and levels off for $\sigma_M > \sigma_M^*$ (Lin *et al.*, 2003).

The markedly different transfection behavior of L_{α}^C CL-DNA complexes at low and high σ_M prompted further investigations with confocal microscopy (Lin *et al.*, 2003). LSCM images of cells transfected with L_{α}^C complexes at high σ_M show a path of complex uptake and DNA release distinct from both L_{α}^C complexes at low σ_M (Fig. 5.6B) and H_{II}^C complexes (Fig. 5.6A). A typical confocal image of a cell incubated for 6 h with L_{α}^C complexes at $M_{DOPC} = 0.18$ ($\sigma_M \approx 0.012 \text{ e/\AA}^2$) is shown in Fig. 5.8. Since there is no indication of transfer of fluorescent lipid to the plasma membrane, the lamellar complexes with high σ_M must have entered the cells through endocytosis, similar to their low- σ_M counterparts. A few intact complexes are visible inside the cell: Fig. 5.8 (label 2; box 2) shows the equal green (DNA) and red (lipid) fluorescence intensity along the dotted line in the inset. In addition, a mass of exogenous DNA successfully transferred into the cytoplasm is evident (Fig. 5.8, label 1: box 1 shows the much larger green (DNA) fluorescence intensity along the x-y diagonal). The integrated fluorescence intensity of the observed DNA (Fig. 5.8, box 1) is comparable to that of DNA complexed with lipids (Fig. 5.8, box 2). This indicates that the released DNA is in the form of aggregates. Since there are no DNA-condensing molecules (Bloomfield, 1991) in the endosome, these aggregates must reside in the cytoplasm. The presence of lipid-free DNA in the cytoplasm after endocytosis of complexes is in agreement with the measured high TE and, moreover, implies fusion between CL-DNA lipids and endosomal membranes, enabling escape from the endosome. The confocal image also shows a large aggregate of complexes in one part of the cell (Fig. 5.8, label 3). Comparing the changes in fluorescence intensity along the x-y diagonal (Fig. 5.8, box 3) and z-axis (Fig. 5.8, box 4), from the outside toward the inside of the cell, we see an aggregate of complexes caught in the process of dissociation after endocytosis, with released DNA toward the inside of the cell.

Since LSCM suggested endocytosis as the mechanism of cell entry for L_{α}^C CL-DNA complexes and DNA appeared trapped within complexes at low σ_M , transfection experiments in the presence of chloroquine were performed. This is a well-established bioassay known to enhance the release of material trapped within endosomes (Felgner, 1990) by osmotically bursting late-stage

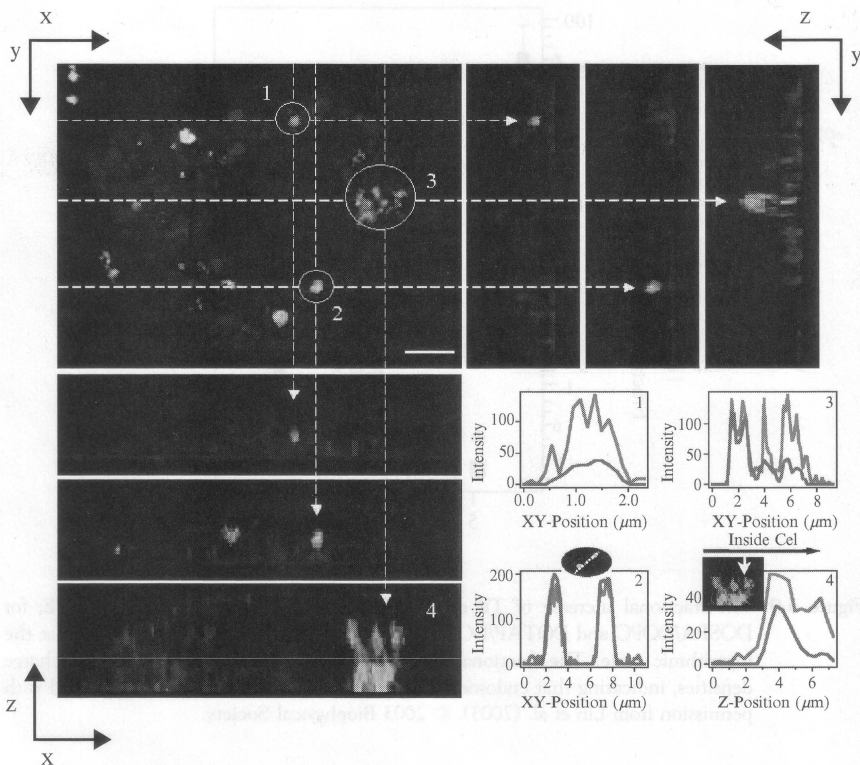
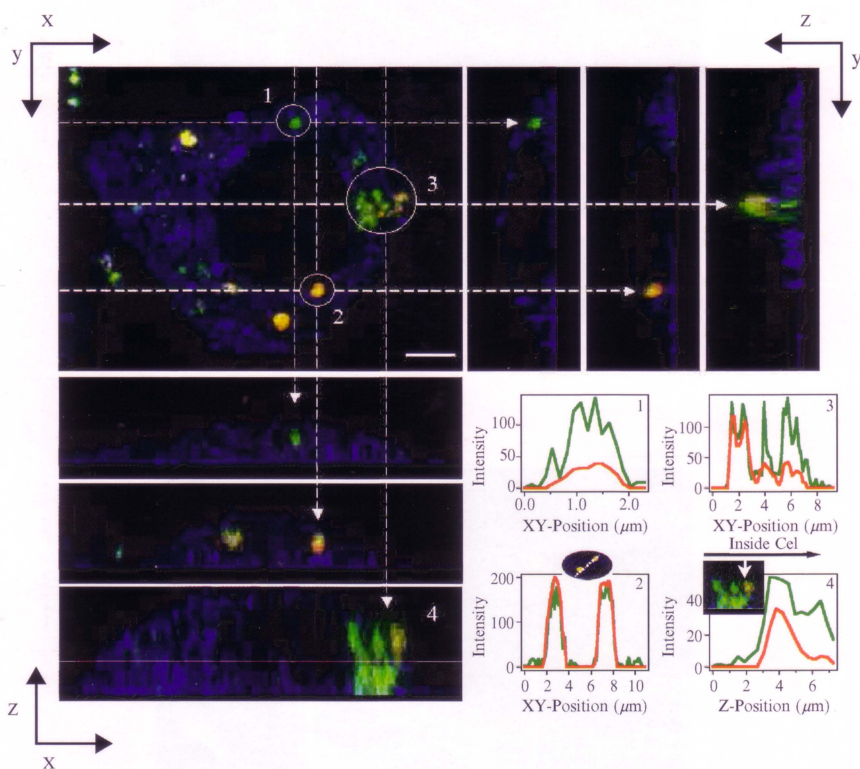


Figure 5.8. A typical LSCM image of a mouse L cell transfected with L_{α}^C complexes at $M_{DOPC} = 0.18$, corresponding to cationic membranes with a high charge density $\sigma_M \approx 0.012 e/\text{\AA}^2$ and high TE (cf. Figure 5.7). Red and green fluorescence corresponds to lipid and DNA labels, respectively; yellow, the overlap of the two, denotes CL–DNA complexes. The cell outline was observed in reflection mode, appearing in blue. Scale bars are $5 \mu\text{m}$. The center image is the x – y (top) view at a given z ; on the right are y – z side views along the vertical dotted lines; at the bottom are x – z side views along the horizontal dotted lines. In the boxes in the lower right corner, plots of lipid and DNA fluorescence intensity along the x – y diagonal or z -axis are shown for objects labeled with numbers. Although the lamellar complexes used here show high TE, no lipid transfer to the cell plasma membrane is seen in contrast to high-transfecting H_{II}^C complexes (Figure 5.6A). Both released DNA (1) and intact complexes (2) are observed inside the cell. Labels (3) and (4): A complex in the process of releasing its DNA into the cytoplasm. Reprinted with permission from Lin *et al.* (2003). © 2003 Biophysical Society. (See Color Insert.)

endosomes. The fractional increase ($TE_{\text{chloroquine}}/TE$; note the logarithmic scale) for the DOSPA/DOPC and DOTAP/DOPC lipid systems with added chloroquine, plotted as a function of σ_M (Fig. 5.9), shows a large increase by as much as a factor of 60 as σ_M decreases. This indicates that lamellar L_{α}^C complexes are trapped within endosomes at low σ_M , consistent both with the



Chapter 5, Figure 5.8. A typical LSCM image of a mouse L cell transfected with L_{α}^C complexes at $m_{\text{DOPC}} = 0.18$, corresponding to cationic membranes with a high charge density $\sigma_M \approx 0.012 \text{ e}/\text{\AA}^2$ and high TE (cf. Figure 5.7). Red and green fluorescence corresponds to lipid and DNA labels, respectively; yellow, the overlap of the two, denotes CL–DNA complexes. The cell outline was observed in reflection mode, appearing in blue. Scale bars are $5 \mu\text{m}$. The center image is the x – y (top) view at a given z ; on the right are y – z side views along the vertical dotted lines; at the bottom are x – z side views along the horizontal dotted lines. In the boxes in the lower right corner, plots of lipid and DNA fluorescence intensity along the x – y diagonal or z -axis are shown for objects labeled with numbers. Although the lamellar complexes used here show high TE, no lipid transfer to the cell plasma membrane is seen in contrast to high-transfecting H_{II}^C complexes (Figure 5.6A). Both released DNA (1) and intact complexes (2) are observed inside the cell. Labels (3) and (4): A complex in the process of releasing its DNA into the cytoplasm. Reprinted with permission from Lin *et al.* (2003). © 2003 Biophysical Society.

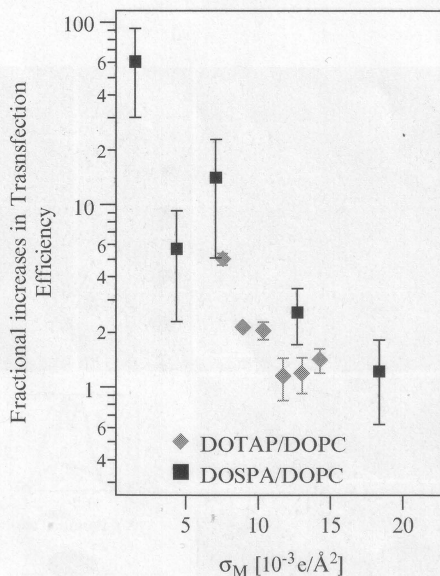


Figure 5.9. The fractional increase of TE upon addition of chloroquine, $TE_{\text{chloroquine}}/TE$, for DOSPA/DOPC and DOTAP/DOPC mixtures, plotted as a function of σ_M . Note the logarithmic scale. The fractional increase is substantial for low membrane charge densities, indicating that endosomal escape is limiting in this regime. Reprinted with permission from Lin *et al.* (2003). © 2003 Biophysical Society.

confocal images (Fig. 5.6B) and the measured low TE without chloroquine. At high σ_M , chloroquine has a much smaller effect on TE, with the fractional increase of order unity. Therefore, endosomal entrapment is not a significant limiting factor in this regime.

C. Transfection properties of new multivalent cationic lipids

To further investigate the finding of a well-defined relationship between transfection efficiency and membrane charge density in lamellar L_α^C complexes, and to more broadly explore the relevance of σ_M as a key chemical parameter, new lipids with multivalent cationic headgroups have been prepared (Ewert *et al.*, 2002; Schulze *et al.*, 1999). Their general structure is shown in Fig. 5.10, and their headgroups are compiled in Table 5.1. The headgroups are derived from the amino acid ornithine. By the addition of 0 to 3 propyl-amine groups, we have generated headgroup charges from +2 (MVL2) to +5 (MVL5). For comparison, a glycine-based monovalent lipid (MVL1) was prepared as well.

Earlier results for one of the lipids (MVL5) showed structurally stable MVL5/DOPC/DNA complexes, forming the L_α^C phase throughout the lipid composition range (Ewert *et al.*, 2002). As depicted in Fig. 5.11, X-ray

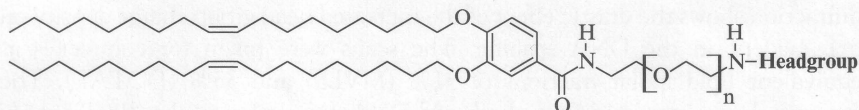


Figure 5.10. General structure of the new, ornithine-based multivalent lipids.

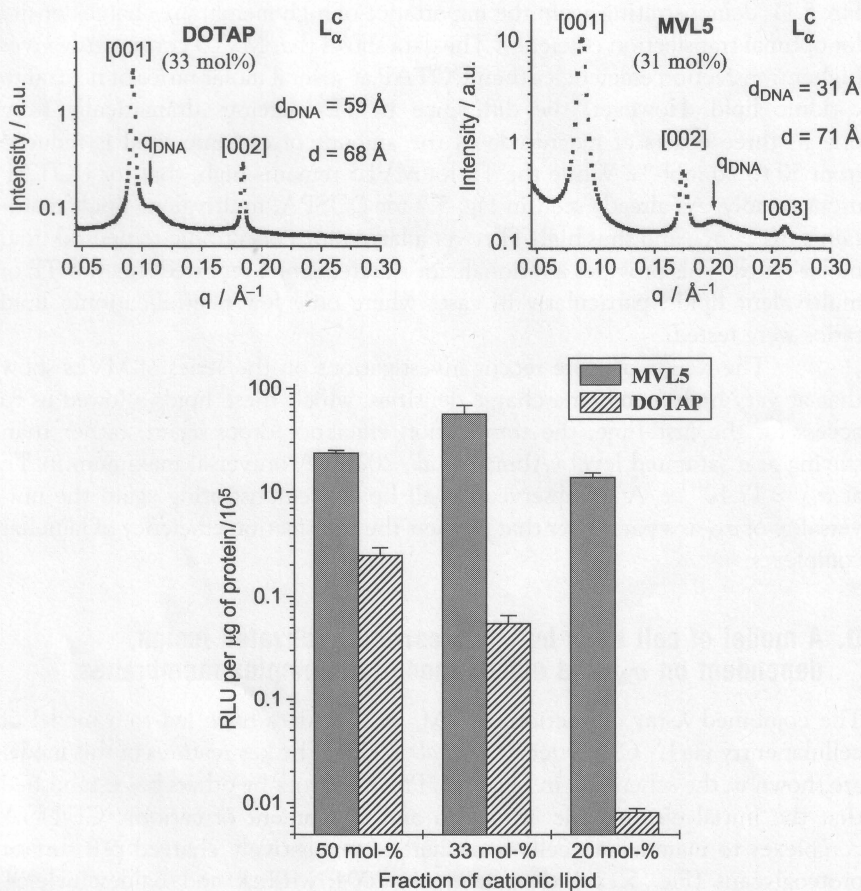


Figure 5.11. Top: Small angle XRD patterns of CL-DNA complexes from MVL5/DOPC and DOTAP/DOPC lipid mixtures at equivalent molar fractions of cationic lipid (31% MVL5; 33% DOTAP; complexes prepared in DMEM). The complexes are in the lamellar phase. The DNA interaxial spacing is reduced from 59 Å in the complexes with DOTAP to 31 Å in the complexes with MVL5, reflecting their higher membrane charge density. Bottom: Transfection efficiencies for cationic lipids DOTAP and MVL5 in mixtures with DOPC. Reprinted with permission from Ewert *et al.* (2002). © 2002 American Chemical Society.

diffraction shows the drastic effect of the increased head group charge density on σ_M , evident in the DNA spacing. The scans were taken for complexes at equivalent lipid molar fractions of 31% (MVL5) and 33% (DOTAP). The spacings d_{DNA} , extracted from the broad DNA correlation peaks (Rädler *et al.*, 1997), are $d_{\text{DNA}} = 2\pi/q_{\text{DNA}} = 31.2 \text{ \AA}$ and $d_{\text{DNA}} = 59.5 \text{ \AA}$ for the complexes prepared with pentavalent MVL5 and univalent DOTAP, respectively. At this composition, the transfection efficiency of the MVL5 complexes is approximately 100-fold higher than that of the DOTAP complexes. This is also shown in Fig. 5.11, demonstrating again the importance of high membrane charge density for optimal transfection efficiency. The data shows that MVL5 consistently gives higher transfection efficiencies than DOTAP at several molar ratios of neutral to cationic lipid. However, the difference in TE increases dramatically from one to three orders of magnitude as the amount of cationic lipid is reduced from 50 to 20 mol-%. While the TE for MVL5 remains high, that for DOTAP drops rapidly. As already seen in Fig. 5.7 for DOSPA, multivalent lipids maintain a $\sigma_M > \sigma_M^*$, and thus high TE, over a large range of cationic to neutral lipid molar ratios. This provides a rationale for the frequently reported superior TE of multivalent lipids, particularly in cases where only few neutral/cationic lipid ratios were tested.

The results of more recent investigations on the series of MVLs show that at very high membrane charge densities, which these lipids allowed us to access for the first time, the transfection efficiency drops again, rather than staying at a saturated level (Ahmad *et al.*, 2005). A universal maximum in TE at $\sigma_M \approx 17.10^{-3} \text{ e/\AA}^2$ is observed for all lipids, demonstrating again the universality of σ_M as a parameter that predicts the transfection efficiency of lamellar complexes.

D. A model of cell entry by L_α^C CL carriers: activated fusion, dependent on σ_M and elastic moduli of complex membranes

The combined X-ray diffraction, LSCM, and TE data have led to a model of cellular entry via L_α^C CL carriers (Lin *et al.*, 2003). The key features of this model are shown in the schematic in Fig. 5.12. Previous work by others has established that the initial electrostatic attraction and attachment of cationic CL-DNA complexes to mammalian cells is mediated by negatively charged cell surface proteoglycans (Fig. 5.12a) (Kopatz *et al.*, 2004; Mislick and Baldeschwieler, 1996; Mounkes *et al.*, 1998). LSCM at room temperature and 4 °C, transfection in the presence of chloroquine as well as the results from other groups indicate that L_α^C complexes enter via the endocytic pathway (Fig. 5.12b,c) (Lin *et al.*, 2003; Wrobel and Collins, 1995; Xu and Szoka 1996; Zabner *et al.* 1995). As seen in LSCM, the further intracellular fate of the complexes strongly depends on their membrane charge density: at low σ_M , complexes remain intact and trapped in the endosomes (Fig. 5.12c), whereas they successfully escape at high

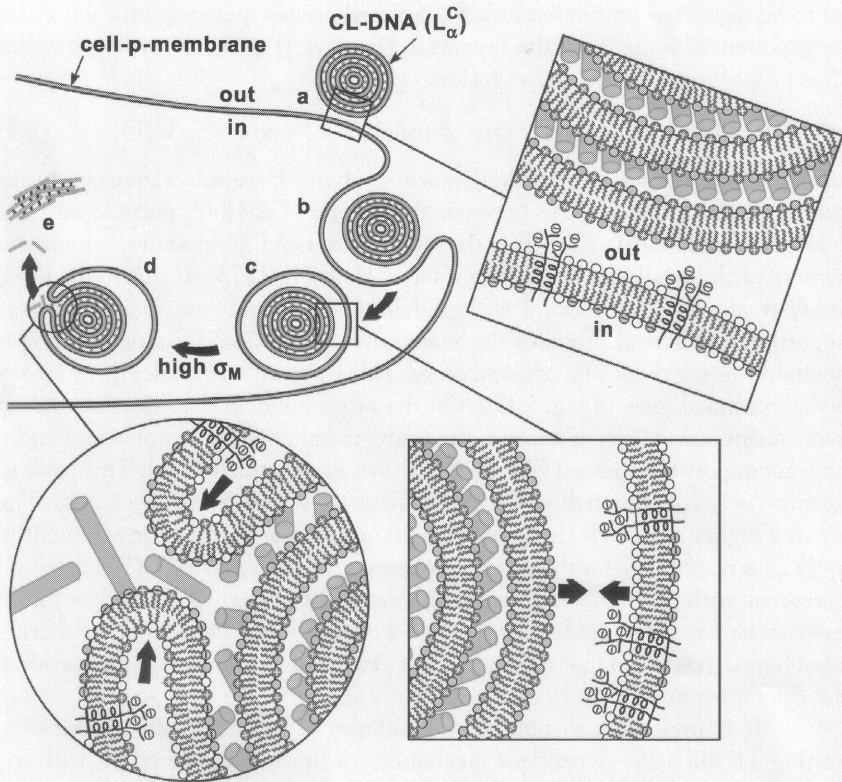
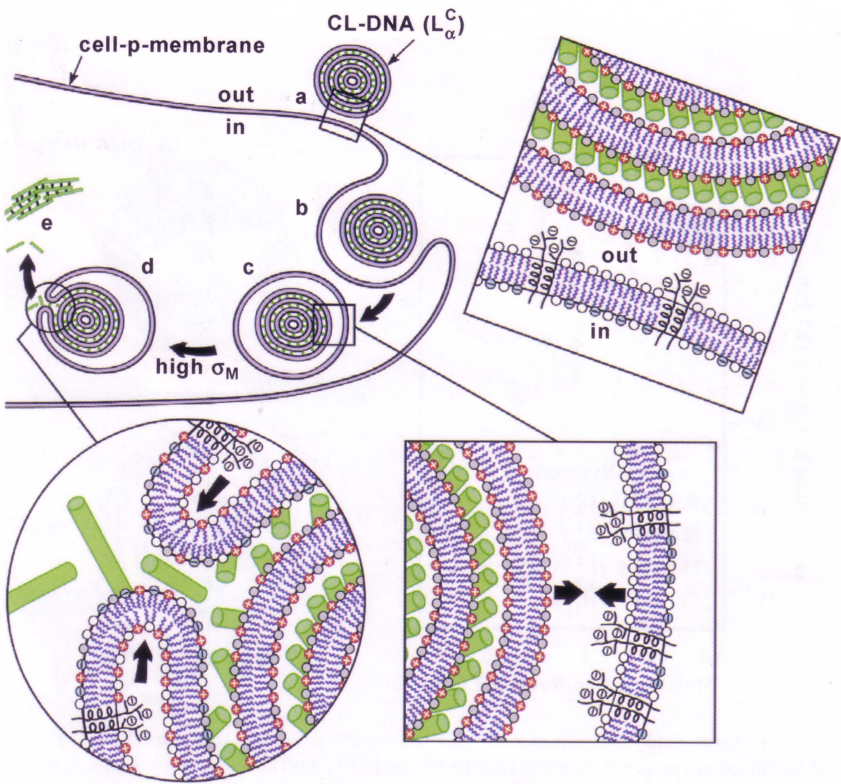


Figure 5.12. Model of cellular uptake and endosomal release (through activated fusion) of L_{α}^C complexes. (a) Cationic complexes adhere to cells due to electrostatic attraction between positively charged CL-DNA complexes and negatively charged cell-surface proteoglycans (shown in expanded views). (b and c) After attachment, complexes enter through endocytosis. (d) Only complexes with sufficiently high membrane charge density escape from the endosome through activated fusion with the endosomal membrane. (e) Confocal microscopy shows that lipid-free DNA inside the cell exists primarily in the form of aggregates. These DNA aggregates must reside in the cytoplasm because oppositely charged cellular biomolecules able to condense DNA are not present in the endosome. Arrows in the expanded view of (c) indicate the electrostatic attraction between the oppositely charged membranes of the complex and endosome, which enhances adhesion and fusion. Arrows in the expanded view of (d) indicate the bending of the membranes required for fusion, which constitutes the main barrier for the process. Reprinted with permission from Lin *et al.* (2003). © 2003 Biophysical Society. (See Color Insert.)

σ_M . Therefore, Lin *et al.* (2003) proposed that escape from the endosome is the process limiting TE for $\sigma_M < \sigma_M^*$. The most likely mechanism for this is through fusion with the endosomal membrane (Fig. 5.12d), with a kinetic barrier that



Chapter 5, Figure 5.12. Model of cellular uptake and endosomal release (through activated fusion) of L_{α}^C complexes. (a) Cationic complexes adhere to cells due to electrostatic attraction between positively charged CL-DNA complexes and negatively charged cell-surface proteoglycans (shown in expanded views). (b and c) After attachment, complexes enter through endocytosis. (d) Only complexes with sufficiently high membrane charge density escape from the endosome through activated fusion with the endosomal membrane. (e) Confocal microscopy shows that lipid-free DNA inside the cell exists primarily in the form of aggregates. These DNA aggregates must reside in the cytoplasm because oppositely charged cellular biomolecules able to condense DNA are not present in the endosome. Arrows in the expanded view of (c) indicate the electrostatic attraction between the oppositely charged membranes of the complex and endosome, which enhances adhesion and fusion. Arrows in the expanded view of (d) indicate the bending of the membranes required for fusion, which constitutes the main barrier for the process. Reprinted with permission from Lin *et al.* (2003). © 2003 Biophysical Society.

has to be overcome (activated fusion). An Arrhenius-type equation then yields the exponential increase of the universal TE curve (Fig. 5.7B) with σ_M , where TE is proportional to the rate of fusion:

$$\text{Transfection Efficiency} \propto \text{rate of fusion} = \tau^{-1}[\exp(-\delta E/k_B T)], \quad (5.2)$$

with $\delta E =$ kinetic energy barrier height $= a \cdot \kappa - b \cdot \sigma_M$. Here, $a, b > 0$ are constants, and τ^{-1} is the collision rate between the trapped CL-DNA particle and the endosomal wall (Fig. 5.12c); κ is the membrane-bending modulus, which is a measure of the flexibility of the membrane (Helfrich, 1973; Israelachvili, 1992; Janiak *et al.*, 1979; Seddon, 1990). Bending of a membrane requires energy proportional to κ and provides the main barrier to fusion, because bending is inevitable during the fusion of membranes. This is shown schematically by arrows in the expanded view of Fig. 5.12d. On the other hand, electrostatic attraction favors membrane adhesion because the fusing membranes of complex and endosome are oppositely charged (Fig. 5.12c, arrows in expanded view). This leads to the term " $-b \cdot \sigma_M$ ", which describes the fact that σ_M lowers the barrier height. The fact that higher σ_M lowers the barrier height and thus appears in the exponent in Eq. (5.2) is responsible for the observed exponential increase of TE (Fig. 5.7b). In agreement with this model, a recent theoretical study, which considers fusion between two neutral lipid bilayers (i.e., pores forming between neighboring membranes), has found that the main energy barrier against fusion is proportional to κ (Gompper and Goos, 1995).

It is important to note that if cellular attachment and uptake were limiting TE via a σ_M -dependent mechanism, a linear increase of TE with σ_M would be predicted. Thus, the TE data, which shows an exponential increase, excludes this possibility. In addition, the observed effect of chloroquine on TE can not be explained by assuming uptake-limited transfection.

E. Transfection properties of inverted hexagonal H_{II}^C complexes

A comparison of TE as a function of σ_M for DOTAP/DOPC-DNA and DOTAP/DOPE-DNA complexes is shown in Fig. 5.13 (left). The DOTAP/DOPE system goes through 2 phase transitions: From L_α^C (filled squares) at high amounts of DOTAP to coexisting $L_\alpha^C + H_{II}^C$ (squares with cross) to H_{II}^C (open squares). In contrast to DOPC containing complexes, for which TE increases exponentially over nearly four decades with increasing $\sigma_M < \sigma_M^*$, the TE of DOPE-containing H_{II}^C complexes is independent of σ_M : at high $M_{DOPE} > 0.56$, DOTAP/DOPE-DNA complexes are in the H_{II}^C phase and continue to exhibit high TE. We can thus conclude that σ_M is an essential parameter for transfection with L_α^C complexes but not H_{II}^C complexes. The mechanism of transfection by DOPE containing H_{II}^C complexes is dominated by other effects as we describe below.

F. A model of cell entry by CL-vectors with the H_{II}^C structure: relevance of the outermost lipid layer

In LSCM, mixing of the lipids of H_{II}^C complexes with the plasma membrane is observed as lipid fluorescence outlining the plasma membrane (Lin *et al.*, 2003). Confocal imaging further shows that the interaction between H_{II}^C complexes and cells leads to release of DNA from the lipid vectors, consistent with their high TE. Therefore, H_{II}^C complexes must undergo rapid fusion with cellular membranes. Fig. 5.13 (right) schematically shows a mechanism that may be responsible for this. The top part (a) pictures a H_{II}^C complex, approaching either the plasma or the endosomal membrane. The cell-surface

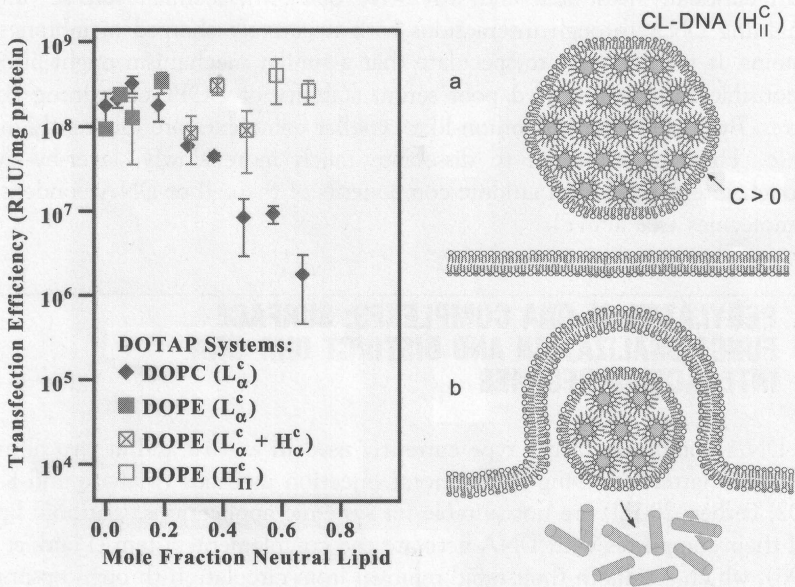
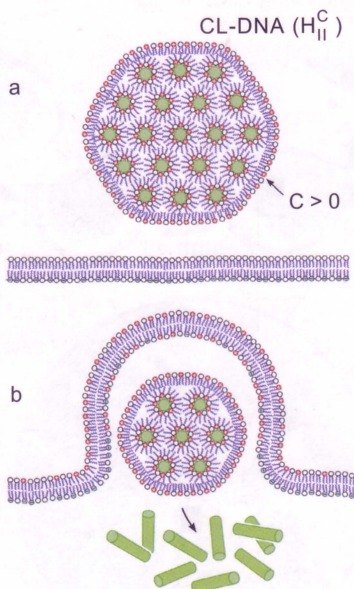
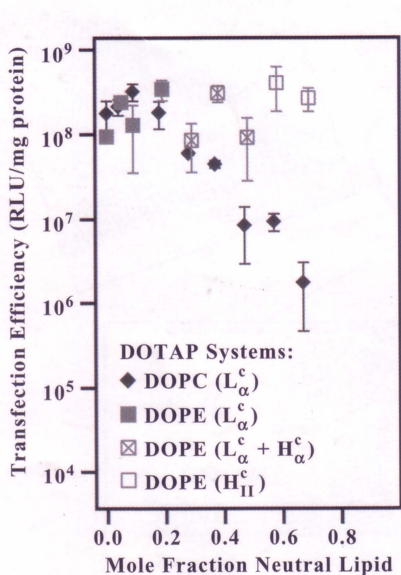


Figure 5.13. Left: TE and complex structure as a function of molar fraction of neutral lipid for complexes prepared from DOTAP/DOPC and DOTAP/DOPE mixtures. Right: Schematic of the proposed mechanism of cell entry/endosomal fusion of inverted hexagonal complexes. An H_{II}^C CL-DNA complex is shown interacting with the plasma membrane or the endosomal membrane. The cell-surface proteoglycans of the cellular membrane have been omitted for clarity. The outer lipid monolayer covering the H_{II}^C CL-DNA complex has a positive curvature. However, the preferred curvature of the lipids forming the complex membrane is negative, as realized in the tubules coating DNA within the complex. Thus, the outer layer is energetically costly. This results in a driving force, independent of the cationic membrane charge density, for rapid fusion of the H_{II}^C complex with the bilayer of the cell plasma membrane or the endosomal membrane. Reprinted with permission from Lin *et al.* (2003). © 2003 Biophysical Society. (See Color Insert.)



Chapter 5, Figure 5.13. Left: TE and complex structure as a function of molar fraction of neutral lipid for complexes prepared from DOTAP/DOPC and DOTAP/DOPE mixtures. Right: Schematic of the proposed mechanism of cell entry/endosomal fusion of inverted hexagonal complexes. An H_{II}^c CL-DNA complex is shown interacting with the plasma membrane or the endosomal membrane. The cell-surface proteoglycans of the cellular membrane have been omitted for clarity. The outer lipid monolayer covering the H_{II}^c CL-DNA complex has a positive curvature. However, the preferred curvature of the lipids forming the complex membrane is negative, as realized in the tubules coating DNA within the complex. Thus, the outer layer is energetically costly. This results in a driving force, independent of the cationic membrane charge density, for rapid fusion of the H_{II}^c complex with the bilayer of the cell plasma membrane or the endosomal membrane. Reprinted with permission from Lin *et al.* (2003). © 2003 Biophysical Society.

proteoglycans, which again mediate the attraction between the complex and the membrane (cf. Fig. 5.12), have been omitted for clarity. The preferred (natural) membrane curvature for lipids forming H_{II}^C complexes is negative, as opposed to ≈ 0 for lipids that form the L_{α}^C structure. Such curvature is realized for the lipids coating DNA inside the H_{II}^C complex, but the curvature of the outermost lipid monolayer, which must cover the H_{II}^C complex to provide a hydrophilic surface, is positive. This elastically frustrated state of the outer monolayer, which is independent of σ_M , drives the rapid fusion with the plasma or endosomal membrane. The fusion releases a layer of DNA and a smaller H_{II}^C complex, as shown in Fig. 5.13 (right, bottom). Speaking in terms of the model for cell entry of L_{α}^C complexes, the activation energy for fusion of H_{II}^C complexes with the endosomal membrane is negligible and this step no longer limits TE. The outer layer of the released, smaller H_{II}^C complex is again elastically frustrated and will drive quick intracellular release of the remaining DNA through interactions with negatively charged membranes or proteins. It is interesting to speculate that a similar mechanism might also be responsible for the observed poor serum stability of DOPE-containing complexes. By comparison, the onion-like lamellar complexes are inherently more stable. They are expected to dissociate much more slowly, layer-by-layer, through interactions with anionic components of the cell or DNA-condensing biomolecules (see above).

IV. PEGYLATED CL-DNA COMPLEXES: SURFACE FUNCTIONALIZATION AND DISTINCT DNA-DNA INTERACTION REGIMES

CL-DNA complexes of the type currently used in *ex vivo* and *in vivo* clinical trials (the latter involving intratumoral injection methods (Mahato and Kim, 2002; Ferber, 2001)) are not suitable for systemic applications. Cationic lipids and their complexes with DNA activate the complement system (Plank *et al.*, 1996), which results in their rapid removal from circulation through opsonization. Poly(ethyleneglycol) (PEG) conjugation to non-viral vectors can reduce the activation of the complement system, as is well known for liposomes (Bradley *et al.*, 1998; Lasic and Martin, 1995; Lasic and Papahadjopoulos, 1995; Woodle, 1995). The presence of a hydrophilic polymeric shell on liposomes provides a repulsive barrier and results in vastly increased circulation lifetimes, a phenomenon referred to as steric stabilization. Thus, incorporating PEG-lipids is an essential step in making CL-DNA complexes a viable option for systemic gene delivery. For future applications, it is also important to have the ability to use polymer chains of variable length as tethers for target-specific ligands (e.g., peptides), which will add functionality and specificity to the

complexes. Therefore, it is crucial to gain an understanding of the effects of incorporating PEG-lipids into CL-DNA complexes.

A. DNA–DNA interaction regimes in PEGylated CL-DNA complexes

Recent experiments in our group have probed the structure, morphology and function of CL-DNA complexes consisting of a ternary mixture of DOTAP, DOPC, and PEG-lipids (Martin-Herranz *et al.*, 2004; Schulze *et al.*, 1999). This work has shown that a critical value of PEG chain length exists, above which steric stabilization and other polymer-specific effects become evident. The structures of the investigated lipids are displayed in Fig. 5.1. X-ray diffraction of isoelectric ($\rho_{\text{chg}} = 1$) complexes revealed one phase of stable complexes with a well-ordered lamellar structure for the PEG400-lipids. The lamellar structure was also observed for the PEG2000-lipids, but phase separation occurs at higher molar ratios of PEG-lipid (>7 mol-% for PEG2000²⁺-lipid; >10 mol-% for PEG2000-lipid). Complete incorporation of PEG-lipid into the complexes is not possible beyond these limits.

The effect of incorporating PEG400²⁺-lipid into isoelectric CL-DNA complexes was studied by monitoring the distance between DNA chains (d_{DNA} ; see Fig. 5.2) while increasing the molar fraction of PEG400²⁺-lipid at various constant molar fractions of DOTAP (M_{DOTAP}). The results reveal that PEG400²⁺-lipid simply acts as a cationic co-lipid, leading to condensation of DNA through an increase in the membrane charge density. As with DOTAP (Salditt *et al.*, 1998), two distinct DNA interaction regimes are observed: in the electrostatic regime ($4 < \sigma_{\text{M}}/10^{-3} \text{ e}/\text{\AA}^2 < 8.5$), d_{DNA} depends purely on the membrane charge density. In the regime of $\sigma_{\text{M}} > 8.5 \cdot 10^{-3} \text{ e}/\text{\AA}^2$, a strong repulsive hydration barrier between DNA rods dominates (Salditt *et al.*, 1998), preventing further condensation of DNA by added PEG400²⁺-lipid. Neutral PEG400-lipid also shows no polymer-specific behavior, its exchange with DOPC resulting in no effect on the DNA spacing.

A distinctly different picture arises for PEG-lipids with chains of molecular weight 2000 g/mol. Fig. 5.14A shows XRD data from single-phase PEG-CL-DNA complexes. Increasing amounts of neutral PEG2000-lipid were added to the membranes of DOTAP/DOPC-DNA complexes at constant $M_{\text{DOTAP}} = 30\%$. The DNA interaxial spacing d_{DNA} ($d_{\text{DNA}} = 2\pi/q_{\text{DNA}}$) decreases from 53.7 Å (0% PEG-lipid) to 49.1 Å (1.6 mol-% PEG-lipid) to 41.6 Å (6.7 mol-% PEG-lipid) with increasing molar fraction of PEG2000-lipid, indicating the existence of an additional attractive force. This attraction is due to the presence of a polymer chain in the confined space between the lipid bilayers where the DNA chains reside (depletion attraction force; see below). The fact that addition of neutral as well as cationic (data not shown) PEG2000-lipid decreases the DNA spacing confirms that the polymer

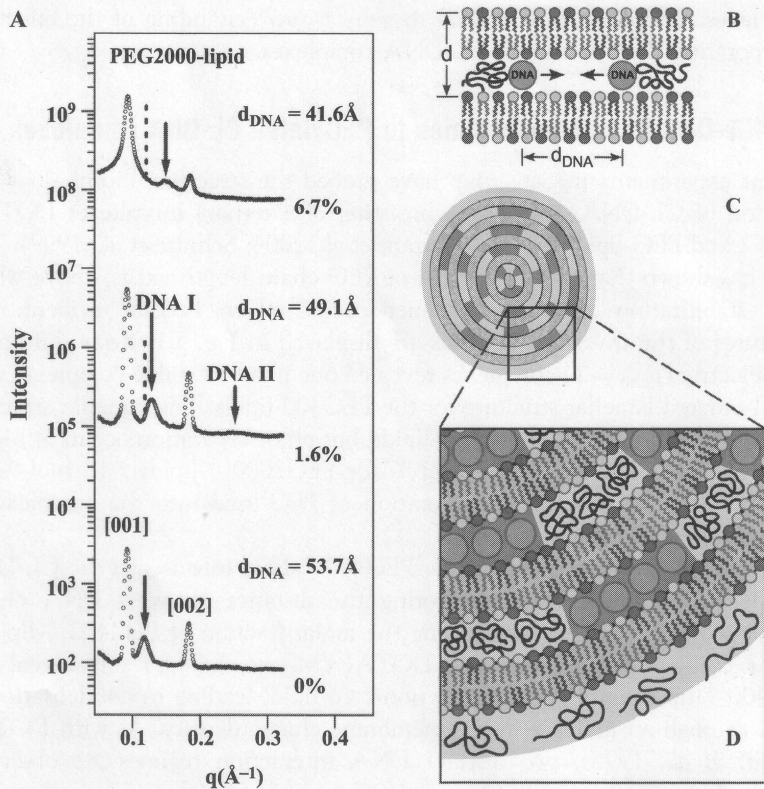


Figure 5.14. (A): XRD scans of L_{α}^C CL-DNA complexes with PEG₂₀₀₀-lipid incorporated within their membranes. Arrows point to the DNA interaxial peak which moves to larger q_{DNA} (corresponding to a decrease of d_{DNA}) as PEG₂₀₀₀-lipid is added to the membranes of the complex. The dashed line marks the position of q_{DNA} for 0% PEG-lipid). (B–D): Schematics of a lamellar CL-DNA complex containing long-chain PEG-lipids. (B) The presence of the polymer is forcing the DNA rods closer together than predicted by electrostatics (depletion attraction force). (C) Cross-section of a PEG-CL-DNA complex with DNA rich domains (dark gray) and polymer rich domains (light gray) in-between lipid bilayers (gray) (D) Enlarged view showing the internal phase separation as well as the outer shell of polymer chains. Reprinted in part with permission from Martin-Herranz *et al.* (2004). © 2004 Biophysical Society.

chain-DNA interaction is the dominating effect of adding PEG₂₀₀₀-lipids, as opposed to electrostatics in the case of PEG₄₀₀-lipids.

Figure 5.14B schematically shows the origin of the polymer-induced depletion attraction force between DNA strands, which is well known in bulk solution (where much larger PEG molecular weights are required) (Vasilevskaya *et al.*, 1995). Since PEG₂₀₀₀ has a radius of gyration of ≈ 35 Å

(Devanand and Selser, 1991; Warriner *et al.*, 1996), the PEG2000 part of the PEG2000-lipid will be excluded from regions between DNA rods (Israelachvili, 1992). This causes a phase separation between the polymer and the DNA within the layers of the complex, as shown schematically in Fig. 5.14C. The decreased DNA spacing then is a result of osmotic stress, exerted on the DNA domains by the PEG2000 chains confined to the outside of these domains, which increases with the concentration of polymer. As depicted in Fig. 5.14D, the resulting complex has DNA-rich domains, shown in dark gray, and polymer-rich domains, shown in light gray.

B. Surface functionalization of CL-DNA complexes with PEG-lipids

Optical microscopy of PEG-CL-DNA complexes at $\rho_{\text{chg}} = 2.8$ and $M_{\text{DOTAP}} = 0.82$ in DMEM was performed to demonstrate coverage of their surface with the PEG-lipids and further pinpoint their distinct, chain length-dependent behavior. Figure 5.15A shows complexes without PEG-lipid. Some degree of aggregation of the complexes is observed, due to the presence of salts in DMEM. Figure 5.15B shows complexes at $M_{\text{PEG400-lipid}} = 10\%$. Again, the aggregation of the complexes is clearly evident. However, complexes prepared using the long-chain PEG-lipid at $M_{\text{PEG2000-lipid}} = 10\%$ exhibit a strong shielding effect of the polymer (Fig. 5.15C). No aggregation of complex particles occurs, due to steric repulsion conferred by the shell of PEG2000-lipid polymer chains of thickness $\approx 35 \text{ \AA}$ (Devanand and Selser, 1991; Warriner *et al.*, 1996). As mentioned earlier, this stabilization is important for developing a viable *in vivo* gene delivery system (Harvie *et al.*, 2000; Pitard *et al.*, 2001; Wheeler *et al.*, 1999).

Figure 5.15D shows transfection results for positively charged PEG-CL-DNA complexes ($\rho_{\text{chg}} = 2.8$). At $M_{\text{DOTAP}} = 0.80$, transfection efficiency is high without PEG-lipid, but the addition of 6 mol-% PEG2000-lipid or PEG2000²⁺-lipid strongly suppresses TE, by about 2 orders of magnitude. This indicates that the electrostatic binding of the cationic CL-DNA complexes to cells is efficiently reduced due to shielding by the PEG2000 polymer coat. In contrast, the addition of cationic or neutral PEG400-lipid only negligibly affects TE, even at 20 mol-% PEG400-lipid. Thus, no shielding occurs with these shorter amphiphiles and the further addition of cationic co-lipid (PEG400²⁺) does not aid transfection in this regime of high σ_{M} , where TE is at a maximum (Lin *et al.*, 2003). Note that 6 and 20 mol-% of PEG2000-lipid and PEG400-lipid, respectively, correspond to an approximately equal total weight of PEG.

In summary, microscopy and transfection experiments show that the PEG-lipid is coating the surfaces of the complexes, whereas X-ray diffraction results clearly demonstrate that the PEG-lipid is also located internally.

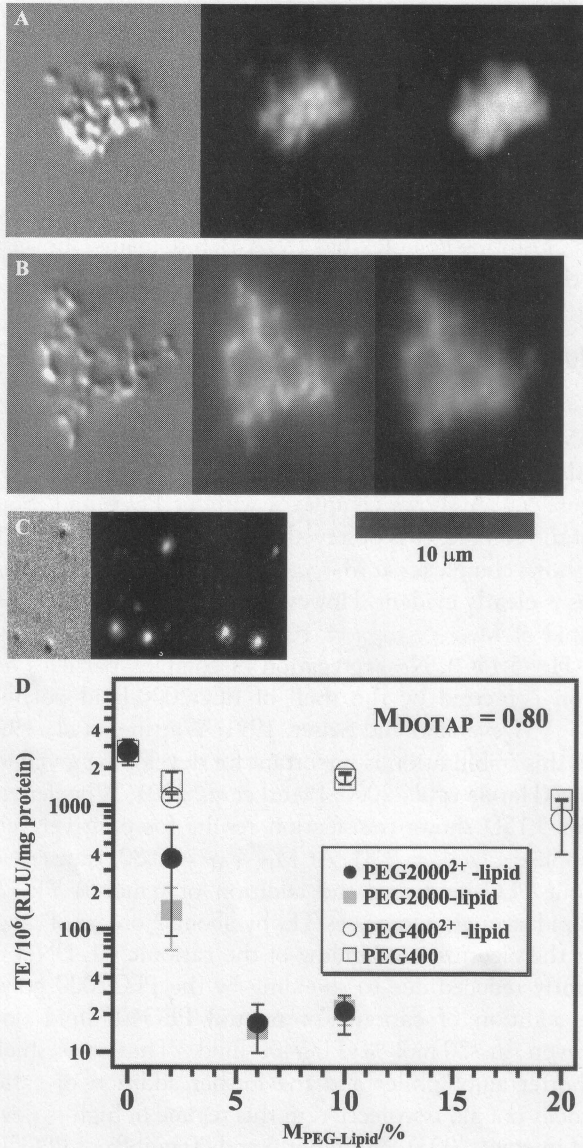


Figure 5.15. (A–C): Microscopy images of DOTAP/DOPC CL–DNA complexes at $M_{\text{DOTAP}} = 0.33$ with plasmid DNA in the presence of DMEM, taken in DIC (left), lipid fluorescence (center) and DNA fluorescence modes. The images show complexes prepared (A) without PEG-lipid, (B) with 10 mol-% PEG400-lipid and (C) with 10 mol-% PEG2000-lipid. The complex particles aggregate when no PEG-lipid or PEG400-lipid are added but are sterically stabilized by 10 mol-% PEG2000-lipid. (D): Transfection efficiency of PEG-lipid/DOTAP/DOPC–DNA complexes as a function of increasing molar fraction of PEG-lipid ($M_{\text{PEG-lipid}}$) added to a DOTAP/

V. CONCLUSION

The structure–function data obtained from the reported work has propelled us further toward the long-term goal of our research: unraveling the mechanisms of transfection of CL-DNA complexes at the molecular to cellular level to enable the rational design of optimal non-viral transfection reagents for gene therapy.

CL-DNA complexes of distinct structure (i.e. L_{α}^C versus H_{II}^C) differ widely in their interactions with cells and their ability to deliver exogenous DNA to the cytoplasm. We have demonstrated that the membrane charge density of the CL-vector, σ_M , is a key universal parameter for transfection with L_{α}^C complexes. The universal TE curve for DOPC-containing L_{α}^C complexes increases exponentially with $\sigma_M < \sigma_M^*$ (the optimal membrane charge density). The TE level of L_{α}^C complexes at σ_M^* is comparable to the high TE of DOPE-containing H_{II}^C complexes, which exhibit no dependence on σ_M . This is an important finding: by not having to rely on DOPE as the neutral lipid in order to induce the H_{II}^C phase, a compositional degree of freedom is gained, and neutral lipids with various functionalities may be introduced while maintaining high TE.

PEG-lipids of various chain lengths are readily incorporated into CL-DNA complexes. The PEG-chains are present on the inside as well as the outside of the complexes, giving rise to polymer-specific effects such as depletion attraction forces between DNA rods and steric stabilization of complex particles above a critical PEG chain length of molecular weight >400 g/mol and ≤ 2000 g/mol. Sterical stabilization achieved by PEG2000-lipids reduces TE significantly but is a necessary first step on the way towards CL-vectors viable for *in vivo* applications.

VI. FUTURE DIRECTIONS

The capabilities of CL-DNA complexes as non-viral vectors and the understanding of their structure and mechanism of action have improved vastly over the last decade. Out of a large variety of lipids and formulations, vectors suitable

DOPC liposome mixture ($M_{DOTAP} = 0.80$ for all complexes). Adding PEG2000²⁺-lipid or PEG2000-lipid leads to a decrease in TE by nearly two orders of magnitude with only 6 mol-% added PEG-lipid. By contrast, addition of PEG400²⁺-lipid or PEG400-lipid does not modify TE significantly, even at 20 mol-% PEG-lipid. As a reference, typical TE for naked DNA is on the order of 300,000 RLU/mg protein. Note that 20 mol-% PEG400-lipid and 6 mol-% PEG2000-lipid correspond to approximately equal total weight of PEG. Reprinted with permission from Martin-Herranz *et al.* (2004). © 2004 Biophysical Society.

for *in vitro* transfection in research settings, some general mechanisms, and a few unifying themes such as the relevance of the membrane charge density have emerged. More such unifying themes are likely to surface, and will help to rationally design more efficient lipids. In standard CL-DNA complexes, the cationic lipids perform multiple functions along the transfection pathway. They condense DNA and provide for electrostatic attachment to the cell surface; they help with escape of the complex from the endosome via activated fusion into the cytoplasm, where they need to dissociate from the DNA. In the future, dividing these responsibilities between several components and enabling specific interactions between complexes and cells, for example, by the incorporation of peptide-ligands, will be an important and exciting avenue of research.

The universality of σ_M as a parameter for transfection by lamellar complexes is best explored with a series of lipids bearing headgroups of systematically varied size and charge (MVLs, Table 5.1). These lipids open access to a new regime of very high membrane charge density. Endosomal escape is not limiting in this regime, which shows an unexpected decrease in TE with increasing σ_M . The full universal curve fits a simple Gaussian bell curve, with an optimal, intermediate membrane charge density σ_M^* resulting from the compromise between the opposing requirements for high TE: higher σ_M improves TE by enhancing the activated fusion with the endosomal membrane, but itself becomes an obstacle to transfection at very high σ_M (Ahmad *et al.*, 2005).

Future studies will also move towards revealing structure-function correlations for transfection *in vivo*. Preparing PEG-coated CL-DNA complexes with strongly reduced electrostatic binding to cells has been a crucial initial step in the development of competent vectors for systemic gene delivery. The next step will be to re-equip these complexes with means of attaching to the targeted cells, preferably via specific, ligand-receptor-based binding. The feasibility of this concept has been demonstrated for liposomes with antibodies as targeting moieties (Allen, 1994), and some work along these lines has also been done with non-viral vectors. However, the need for a thorough and systematic mechanistic investigation has not been met.

Currently, a major continuing focus of work on non-viral gene delivery systems is on optimizing transfection at the cell level in continuous (dividing) cell lines with potential relevance for the clinical development of cancer vaccines (Ferber, 2001; Mahato and Kim, 2002; Nabel *et al.*, 1993; Rinehart *et al.*, 1997; Stopeck *et al.*, 1998). Since the nuclear membrane dissolves during mitosis, it is not a major barrier for delivery and expression of DNA in these experiments (Mortimer *et al.*, 1999). However, even cancer cells are dividing much more slowly than the cells used for *in vitro* experiments

and some very interesting target cells for gene delivery, such as nerve cells, are non-dividing cells. Thus, optimizing TE for complexes that can cross the nuclear membrane is of great interest. This constitutes another application for functionalized CL-DNA complexes, since the nucleus may be targeted with a nuclear localization sequence (NLS) (Jans *et al.*, 1998; Kalderon *et al.*, 1984). Existing work employing NLS peptides to non-viral gene delivery is still ambiguous, and systematic mechanistic studies are lacking (Cartier and Reszka, 2002; Escriou *et al.*, 2003; Hebert, 2003).

Another future avenue of research is exploiting the predictions of our current model of transfection by lamellar complexes. In this model, TE is limited by the rate of the activated fusion of the oppositely charged membranes of CL-DNA complexes and endosome (Ewert *et al.*, 2002; Lin *et al.*, 2003). Since the elastic cost of fusion provides the main barrier for this process, the model suggests that softening of the membranes of CL-DNA complexes should enhance transfection efficiency. The bending modulus of membranes κ scales with lipid chain length l and the area per lipid chain A_L as $\kappa \propto l^3/A_L^5$ (Safinya *et al.*, 1989; Szleifer *et al.*, 1990). Thus, the effect of κ on the TE of CL-DNA complexes can be probed by using lipids of varied chain length.

We can only briefly mention several other exciting new directions in the research on lipid-mediated delivery of nucleic acids here, such as imaging of the transfection process in live cells. Cholesterol has become a highly popular choice of neutral co-lipid and a thorough investigation of its effects on the properties of CL-DNA complexes is required. A rapidly growing and important field is that of delivering small interfering RNA (siRNA). Simultaneously, an ongoing long term objective is to improve efficiency for delivering large pieces of DNA containing human genes and their regulatory sequences (>100 kbp). With such a broad range of cargo, a diversification of vectors, tailored to their respective delivery tasks, seems a logical consequence. Lipid vectors, with their great compositional variability and fundamentally unlimited capacity, are ideally suited for these challenges.

VII. MAIN ABBREVIATIONS

CL	Cationic liposome
DDAB	Didodecyl dimethyl ammonium bromide
DLPC	1,2-Dilauroyl- <i>sn</i> -glycerophosphatidylcholine
DMEM	Dulbecco's modified Eagle's medium
DMRIE	2,3-Di(myristyloxy)propyl(2-hydroxyethyl) dimethylammonium bromide

DOPC	1,2-Dioleoyl- <i>sn</i> -glycerophosphatidylcholine
DOPE	1,2-Dioleoyl- <i>sn</i> -glycerophosphatidylethanolamine
DOSPA	2,3-Dioleyloxy- <i>N</i> -[2-(sperminecarboxamido)ethyl]- <i>N,N</i> -dimethyl-1-propylammonium chloride
DOTAP	2,3-Dioleyloxypropyltrimethylammonium chloride
H _{II} ^C	Inverted hexagonal phase of lipid-DNA complexes
LSCM	Laser scanning confocal microscopy
L _α ^C	Lamellar phase of lipid-DNA complexes
MVL	Multivalent lipid
MVL5	N1-[2-((1S)-1-[(3-Aminopropyl)amino]-4-[di(3-aminopropyl)-amino] butyl-carbox-amido)ethyl]-3,4-di[oleyl]oxy]-benzamide
NLS	Nuclear localization sequence
PEG	Poly(ethylene glycol)
PGA	Poly(L-glutamic acid)
RLU	Relative light units
TE	Transfection efficiency
XRD	X-ray diffraction
κ	Membrane bending rigidity
σ_M	Membrane charge density

Acknowledgments

We gratefully acknowledge useful discussions with Charles Samuel, Cyril George, Robijn Bruinsma and Avinoam Ben-Shaul. We have also benefited over the years through extensive discussions with Phillip Felgner and Leaf Huang. The reported work was supported by grant GM-59288 on DNA-lipid gene delivery studies from the National Institute of General Medical Sciences of the National Institute of Health. Support for the structure studies was also provided by the National Science Foundation DMR 0203755. DOSPA and DMRIE were gifts from Phillip Felgner for which we are grateful. The synchrotron X-ray diffraction experiments were carried out at the Stanford Synchrotron Radiation Laboratory, which is supported by the U.S. Department of Energy. This work made use of MRL Central Facilities supported by the MRSEC Program of the National Science Foundation under award No. DMR00-80034.

References

- Ahmad, A., Evans, H. M., Ewert, K., George, C. X., Samuel, C. E., and Safinya, C. R. (2005). New multivalent lipids reveal bell curve for transfection versus membrane charge density: Non-viral lipid-DNA complexes for gene delivery. *J. Gene Med.* **7**, in press.
- Allen, T. M. (1994). Long-circulating (sterically stabilized) liposomes for targeted drug-delivery. *Trends Pharmacol. Sci.* **15**, 215–220.
- Bloomfield, V. A. (1991). Condensation of DNA by multivalent cations: Considerations on mechanism. *Biopolymers* **31**, 1471–1481.

- Bradley, A. J., Devine, D. V., Ansell, S. M., Janzen, J., and Brooks, D. E. (1998). Inhibition of liposome-induced complement activation by incorporated poly(ethylene glycol) lipids. *Arch. Biochem. Biophys.* **357**, 185–194.
- Bruinsma, R. (1998). Electrostatics of DNA cationic lipid complexes: Isoelectric instability. *Eur. Phys. J. B* **4**, 75–88.
- Cartier, R., and Reszka, R. (2002). Utilization of synthetic peptides containing nuclear localization signals for non-viral gene transfer systems. *Gene Ther.* **9**, 157–167.
- Cavazzana-Calvo, M., Hacein-Bey, S., de Saint Basile, G., Gross, F., Yvon, E., Nusbaum, P., Selz, F., Hue, C., Certain, S., Casanova, J. L., Bousso, P., Le Deist, F., and Fischer, A. (2000). Gene therapy of human severe combined immunodeficiency (SCID)-X1 disease. *Science* **288**, 669–672.
- Chesnoy, S., and Huang, L. (2000). Structure and function of lipid-DNA complexes for gene delivery. *Annu. Rev. Biophys. Biomol. Struct.* **29**, 27–47.
- Clark, P. R., and Hersh, E. M. (1999). Cationic lipid-mediated gene transfer: Current concepts. *Curr. Opin. Mol. Ther.* **1**, 158–176.
- De Smedt, S. C., Demeester, J., and Hennink, W. E. (2000). Cationic polymer-based gene delivery systems. *Pharm. Res.* **17**, 113–126.
- Devanand, K., and Selser, J. C. (1991). Asymptotic-behavior and long-range interactions in aqueous-solutions of poly(ethylene oxide). *Macromolecules* **24**, 5943–5947.
- Edelstein, M. L., Abedi, M. R., Wixon, J., and Edelstein, R. M. (2004). Gene therapy clinical trials worldwide 1989–2004—an overview. *J. Gene Med.* **6**, 597–602.
- Escriou, V., Carriere, M., Scherman, D., and Wils, P. (2003). NLS bioconjugates for targeting therapeutic genes to the nucleus. *Adv. Drug Deliv. Rev.* **55**, 295–306.
- Ewert, K., Ahmad, A., Evans, H. M., Schmidt, H.-W., and Safinya, C. R. (2002). Efficient synthesis and cell-transfection properties of a new multivalent cationic lipid for non-viral gene delivery. *J. Med. Chem.* **45**, 5023–5029.
- Ewert, K., Slack, N. L., Ahmad, A., Evans, H. M., Lin, A. J., Samuel, C. E., and Safinya, C. R. (2004). Cationic lipid-DNA complexes for gene therapy: Understanding the relationship between complex structure and gene delivery pathways at the molecular level. *Curr. Med. Chem.* **11**, 133–149 and other recent reviews in this issue of *Curr. Med. Chem.* 133–220.
- Farhood, H., Serbina, N., and Huang, L. (1995). The role of dioleoyl phosphatidylethanolamine in cationic liposome mediated gene transfer. *Biochim. Biophys. Acta* **1235**, 289–295.
- Felgner, P. L., Gadek, T. R., Holm, M., Roman, R., Chan, H. W., Wenz, W., Northrop, J. P., Ringold, G. M., and Danielsen, M. (1987). Lipofection: A highly efficient, lipid-mediated DNA-transfection procedure. *Proc. Natl. Acad. Sci. USA* **84**, 7413–7417.
- Felgner, P. L. (1990). Particulate systems and polymers for *in vitro* and *in vivo* delivery of polynucleotides. *Adv. Drug Deliv. Rev.* **5**, 163–187.
- Felgner, P. L., and Rhodes, G. (1991). Gene therapeutics. *Nature* **349**, 351–352.
- Ferber, D. (2001). Gene therapy: Safer and virus-free? *Science* **294**, 1638–1642.
- Friedmann, T. (1997). Overcoming the obstacles to gene therapy. *Sci. Am.* **276**, 96–101.
- Gompper, G., and Goos, J. (1995). Fluctuations and phase behavior of passages in a stack of fluid membranes. *J. Phys. II (France)* **5**, 621–634.
- Gruner, S. M., Tate, M. W., Kirk, G. L., So, P. T. C., Turner, D. C., Keane, D. T., Tilcock, C. P. S., and Cullis, P. R. (1988). X-ray-diffraction study of the polymorphic behavior of N-methylated dioleoylphosphatidylethanolamine. *Biochemistry* **27**, 2853–2866.
- Hacein-Bey-Abina, S., von Kalle, C., Schmidt, M., Le Deist, F., Wulfraat, N., McIntyre, E., Radford, I., Villeval, J. L., Fraser, C. C., Cavazzana-Calvo, M., and Fischer, A. (2003a). A serious adverse event after successful gene therapy for X-linked severe combined immunodeficiency. *N. Engl. J. Med.* **348**, 255–256.

- Hacein-Bey-Abina, S., von Kalle, C., Schmidt, M., McCormack, M. P., Wulffraat, N., Leboulch, P., *et al.* (2003b). LMO2-associated clonal T cell proliferation in two patients after gene therapy for SCID-X1. *Science* **302**, 415–419.
- Harries, D., May, S., Gelbart, W. M., and Ben-Shaul, A. (1998). Structure, stability, and thermodynamics of lamellar DNA-lipid complexes. *Biophys. J.* **75**, 159–173.
- Harrington, J. J., van Bokkelen, G., Mays, R. W., Gustashaw, K., and Willard, H. F. (1997). Formation of *de novo* centromeres and construction of first-generation human artificial microchromosomes. *Nat. Genet.* **15**, 345–355.
- Harvie, P., Wong, F. M. P., and Bally, M. B. (2000). Use of poly(ethylene glycol)-lipid conjugates to regulate the surface attributes and transfection activity of lipid-DNA particles. *J. Pharm. Sci.* **89**, 652–663.
- Hebert, E. (2003). Improvement of exogenous DNA nuclear importation by nuclear localization signal-bearing vectors: A promising way for non-viral gene therapy? *Biol. Cell* **95**, 59–68.
- Helfrich, W. (1973). Elastic properties of lipid bilayers: Theory and possible experiments. *Z. Naturforsch.* **28c**, 693–703.
- Henry, C. M. (2001). Gene delivery—without viruses. *Chem. Eng. News* **79**, 35–41.
- Huang, L., Hung, M.-C., and Wagner, E. (eds.) (1999). “Non-viral Vectors for Gene Therapy.” Academic Press, San Diego.
- Hui, S., Langner, M., Zhao, Y., Ross, P., Hurley, E., and Chan, K. (1996). The role of helper lipids in cationic liposome-mediated gene transfer. *Biophys. J.* **71**, 590–599.
- Israelachvili, J. N. (1992). “Intermolecular and Surface Forces.” Academic Press, London.
- Janiak, M. J., Small, D. M., and Shipley, G. G. (1979). Temperature and compositional dependence of the structure of hydrated dimyristoyl lecithin. *J. Biol. Chem.* **254**, 6068–6078.
- Jans, D. A., Chan, C. K., and Hübner, S. (1998). Signals mediating nuclear targeting and their regulation: Application in drug delivery. *Med. Res. Rev.* **18**, 189–223.
- Kalderon, D., Roberts, B. L., Richardson, W. D., and Smith, A. E. (1984). A short amino acid sequence able to specify nuclear localization. *Cell* **39**, 499–509.
- Koltover, I., Salditt, T., Rädler, J. O., and Safinya, C. R. (1998). An inverted hexagonal phase of cationic liposome-DNA complexes related to DNA release and delivery. *Science* **281**, 78–81.
- Koltover, I., Salditt, T., and Safinya, C. R. (1999). Phase diagram, stability and overcharging of lamellar cationic lipid—DNA self-assembled complexes. *Biophys. J.* **77**, 915–924.
- Koltover, I., Wagner, K., and Safinya, C. R. (2000). DNA condensation in two dimensions. *Proc. Natl. Acad. Sci. USA* **97**, 14046–14052.
- Kopatz, I., Remy, J.-S., and Behr, J.-P. (2004). A model for non-viral gene delivery: Through syndecan adhesion molecules and powered by actin. *J. Gene Med.* **6**, 769–776.
- Kumar, V. V., Singh, R. S., and Chaudhuri, A. (2003). Cationic transfection lipids in gene therapy: Successes, setbacks, challenges and promises. *Curr. Med. Chem.* **10**, 1297–1306 and the other recent reviews in this issue of *Curr. Med. Chem.* 1185–1315.
- Lasic, D. D., and Martin, F. J. (eds.) (1995). “Stealth Liposomes.” CRC Press, Boca Raton.
- Lasic, D. D., and Papahadjopoulos, D. (1995). Liposomes revisited. *Science* **267**, 1275–1276.
- Lasic, D. D., Strey, H., Stuart, M. C. A., Podgornik, R., and Frederik, P. M. (1997). The structure of DNA-liposome complexes. *J. Am. Chem. Soc.* **119**, 832–833.
- Le Bret, M., and Zimm, B. H. (1984). Distribution of counterions around a cylindrical polyelectrolyte and Manning’s condensation theory. *Biopolymers* **23**, 287–312.
- Lin, A. J., Slack, N. L., Ahmad, A., Koltover, I., George, C. X., Samuel, C. E., and Safinya, C. R. (2000). Structure–function studies of lipid-DNA non-viral gene delivery systems. *J. Drug Targeting* **8**, 13–27.
- Lin, A. J., Slack, N. L., Ahmad, A., George, C. X., Samuel, C. E., and Safinya, C. R. (2003). Three-dimensional imaging of lipid gene-carriers: Membrane charge density controls

- universal transfection behavior in lamellar cationic liposome-DNA complexes. *Biophys. J.* **84**, 3307–3316.
- Mahato, R. L., and Kim, S. W. (eds.) (2002). "Pharmaceutical Perspectives of Nucleic Acid-Based Therapeutics." Taylor & Francis, London.
- Manning, G. S. (1978). Limiting laws and counterion condensation in polyelectrolyte solutions. I. Colligative properties. *J. Chem. Phys.* **51**, 924–933.
- Martin-Herranz, A., Ahmad, A., Evans, H. M., Ewert, K., Schulze, U., and Safinya, C. R. (2004). Surface functionalized cationic lipid-DNA complexes for gene delivery: PEG-ylated lamellar complexes exhibit distinct DNA-DNA interaction regimes. *Biophys. J.* **86**, 1160.
- May, S., and Ben-Shaul, A. (2004). Modeling of cationic lipid-DNA complexes. *Curr. Med. Chem.* **11**, 151–167.
- Miller, A. D. (1998). Cationic liposomes for gene therapy. *Angew. Chem., Int. Ed.* **37**, 1768–1785.
- Miller, A. D. (2003). The Problem with cationic liposome/micelle-based non-viral vector systems for gene therapy. *Curr. Med. Chem.* **10**, 1195–1211.
- Mislick, K. A., and Baldeschwieler, J. D. (1996). Evidence for the role of proteoglycans in cation-mediated gene transfer. *Proc. Natl. Acad. Sci. USA* **93**, 12349–12354.
- Mortimer, I., Tam, P., Maclachlan, I., Graham, R. W., Saravolac, E. G., and Joshi, P. B. (1999). Cationic lipid-mediated transfection of cells in culture requires mitotic activity. *Gene Ther.* **6**, 403–411.
- Mounkes, L. C., Zhong, W., Ciprespalacin, G., Heath, T. D., and Debs, R. J. (1998). Proteoglycans mediate cationic liposome-DNA complex-based gene delivery *in vitro* and *in vivo*. *J. Biol. Chem.* **273**, 26164–26170.
- Nabel, G., Nabel, E., Yang, Z.-Y., Fox, B. A., Plautz, G. E., Gao, X., Huang, L., Shu, S., Gordon, D., and Chang, A. E. (1993). Direct gene transfer with DNA-liposome complexes in melanoma: Expression, biologic activity, and lack of toxicity in humans. *Proc. Natl. Acad. Sci. USA* **90**, 11307–11311.
- Niidome, T., and Huang, L. (2002). Gene therapy progress and prospects: Non-viral vectors. *Gene Ther.* **9**, 1647–1652.
- Pitard, B., Oudrhiri, N., Lambert, O., Vivien, E., Masson, C., Wetzter, B., Hauchecorne, M., Scherman, D., Rigaud, J.-L., Vigneron, J.-P., Lehn, J.-M., and Lehn, P. (2001). Sterically stabilized BGTC-based lipoplexes: Structural features and gene transfection into the mouse airways *in vivo*. *J. Gene Med.* **3**, 478–487.
- Plank, C., Mechtler, K., Szoka, F. C., and Wagner, E. (1996). Activation of the complement system by synthetic DNA complexes, a potential barrier for intravenous gene delivery. *Human Gene Ther.* **7**, 1437–1446.
- Rädler, J. O., Koltover, I., Salditt, T., and Safinya, C. R. (1997). Structure of DNA-cationic liposome complexes: DNA intercalation in multilamellar membranes in distinct interhelical packing regimes. *Science* **275**, 810–814.
- Raper, S. E., Chirmule, N., Lee, F. S., Wivel, N. A., Bagg, A., Gao, G. P., Wilson, J. M., and Batshaw, M. L. (2003). Fatal systemic inflammatory response syndrome in an ornithine transcarbamylase-deficient patient following adenoviral gene transfer. *Mol. Genet. Metab.* **80**, 148–158.
- Remy, J.-S., Sirlin, C., Vierling, P., and Behr, J.-P. (1994). Gene transfer with a series of lipophilic DNA-binding molecules. *Bioconjugate Chem.* **5**, 647–654.
- Rinehart, J., Hersh, E., Issell, B., Triozzi, P., Buhles, W., and Neidhart, J. (1997). Phase 1 trial of recombinant human interleukin-1-beta (rhIL-1-beta), carboplatin, and etoposide in patients with solid cancers: Southwest Oncology Group Study 8940. *Cancer Invest.* **15**, 403–410.
- Safinya, C. R. (2001). Structures of lipid-DNA complexes: Supramolecular assembly and gene delivery. *Curr. Opin. Struct. Biol.* **11**, 440–448.

- Safinya, C. R., and Koltover, I. (1999). Self assembled structures of lipid-DNA non-viral gene delivery systems from synchrotron X-ray diffraction. In "Non-Viral Vectors for Gene Therapy" (L. Huang, M.-C. Hung, and E. Wagner, eds.), pp. 92–117. Academic Press, San Diego.
- Safinya, C. R., Sirota, E. B., Roux, D., and Smith, G. S. (1989). Universality in interacting membranes: The effect of cosurfactants on the interfacial rigidity. *Phys. Rev. Lett.* **62**, 1134–1137.
- Safinya, C. R., Slack, N. L., Lin, A. J., and Koltover, I. (2002). Cationic lipid-DNA complexes for gene delivery: Structure-function correlations. In "Pharmaceutical Perspectives of Nucleic Acid-Based Therapeutics" (R. I. Mahato and S. W. Kim, eds.), pp. 190–209. Taylor & Francis, London.
- Salditt, T., Koltover, I., Rädler, J. O., and Safinya, C. R. (1997). Two-dimensional smectic ordering of linear DNA chains in self-assembled DNA-cationic liposome mixtures. *Phys. Rev. Lett.* **79**, 2582–2585.
- Salditt, T., Koltover, I., Rädler, J. O., and Safinya, C. R. (1998). Self-assembled DNA-cationic-lipid complexes: Two-dimensional smectic ordering, correlations, and interactions. *Phys. Rev. E* **58**, 889–904.
- Schulze, U., Schmidt, H.-W., and Safinya, C. R. (1999). Synthesis of novel cationic poly(ethylene glycol) containing lipids. *Bioconjugate Chem.* **10**, 548–552.
- Seddon, J. M. (1990). Structure of the inverted hexagonal (HII) phase, and non-lamellar phase transitions of lipids. *Biochim. Biophys. Acta* **1031**, 1–69.
- Stopeck, A. T., Hersh, E. M., Brailey, J. L., Clark, P. R., Norman, J., and Parker, S. E. (1998). Transfection of primary tumor cells and tumor cell lines with plasmid DNA/lipid complexes. *Cancer Gene Ther.* **5**, 119–126.
- Subramanian, G., Hjelm, R. P., Deming, T. J., Smith, G. S., Li, Y., and Safinya, C. R. (2000). Structure of complexes of cationic lipids and poly(glutamic acid) polypeptides: A pinched lamellar phase. *J. Am. Chem. Soc.* **122**, 26–34.
- Szleifer, I., Ben-Shaul, A., and Gelbart, W. M. (1990). Chain packing statistics and thermodynamics of amphiphile monolayers. *J. Phys. Chem.* **94**, 5081–5089.
- Tranchant, I., Thompson, B., Nicolazzi, C., Mignet, N., and Scherman, D. (2004). Physicochemical optimization of plasmid delivery by cationic lipids. *J. Gene Med.* **6**, S24–S35.
- Tristram-Nagle, S., Petrache, H. I., and Nagle, J. F. (1998). Structure and interactions of fully hydrated dioleoylphosphatidylcholine bilayers. *Biophys. J.* **75**, 917–925.
- Vasilevskaya, V. V., Khokhlov, A. R., Matsuzawa, Y., and Yoshikawa, K. (1995). Collapse of single DNA molecule in poly(ethylene glycol) solutions. *J. Chem. Phys.* **102**, 6595–6602.
- Wagner, E. (2004). Strategies to improve DNA polyplexes for *in vivo* gene transfer: Will "Artificial Viruses" be the answer? *Pharm. Res.* **21**, 8–14.
- Warriner, H. E., Idziak, S. H. J., Slack, N. L., Davidson, P., and Safinya, C. R. (1996). Lamellar biogels: Fluid-membrane-based hydrogels containing polymer lipids. *Science* **271**, 969–973.
- Wheeler, J. J., Palmer, L., Ossanlou, M., MacLachlan, I., Graham, R. W., Zhang, Y. P., Hope, M. J., Scherrer, P., and Cullis, P. R. (1999). Stabilized plasmid-lipid particles: Construction and characterization. *Gene Ther.* **6**, 271–281.
- Willard, H. F. (2000). Genomics and gene therapy: Artificial chromosomes coming to life. *Science* **290**, 1308–1309.
- Wolff, J. A. (ed.) (1994). "Gene Therapeutics: Methods and Applications of Direct Gene Transfer." Birkhäuser, Boston.
- Wong, G. C. L., Tang, J. X., Lin, A. J., Li, Y., Janmey, P. A., and Safinya, C. R. (2000). Hierarchical self-assembly of F-Actin and cationic lipid complexes: Stacked three-layer tubule networks. *Science* **288**, 2035–2039.

- Woodle, M. C. (1995). Sterically stabilized liposome therapeutics. *Adv. Drug Deliv. Rev.* **16**, 249–265.
- Wrobel, I., and Collins, D. (1995). Fusion of cationic liposomes with mammalian cells occurs after endocytosis. *Biochim. Biophys. Acta* **1235**, 296–304.
- Xu, Y. H., and Szoka, F. C. (1996). Mechanism of DNA release from cationic liposome/DNA complexes used in cell transfection. *Biochemistry* **35**, 5616–5623.
- Zabner, J., Fasbender, A. J., Moninger, T., Poellinger, K. A., and Welsh, M. J. (1995). Cellular and molecular barriers to gene transfer by a cationic lipid. *J. Biol. Chem.* **270**, 18997–19007.